Boletín Geológico

SERVICIO GEOLÓGICO COLOMBIANO

Boletín Geológico, 46, 51–94, 2020
https://doi.org/10.32685/0120-1425/boletingeo.46.2020.535

Received: October 10, 2019
Accepted: January 17, 2020
Published online: June 30, 2020

Volcanism of the La Quinta Formation in the Perijá mountain range

Vulcanismo de la Formación La Quinta en la serranía del Perijá

Gabriel **Rodríguez García** and Gloria **Obando**[1]

1 Servicio Geológico Colombiano.

Email: grodriguez@sgc.gov.co

Abstract

This study reports new data on the petrography, total rock chemistry and U-Pb zircon geochronology of volcanic rocks of the La Quinta Formation that outcrop the western flank of the Perijá mountain range and the Cesar and La Guajira departments. The volcanic rocks consist of basaltic, andesitic, dacitic and rhyolitic lavas, and the volcaniclastic rocks consist of crystal-vitric and crystal-lithic tuffs and agglomerates of calc-alkaline affinity, formed in a continental margin arc setting. Geochronological data suggest that the La Quinta Formation was volcanically active for approximately 25 Ma, during which its composition varied from basaltic trachyandesites to rhyolites. U-Pb dating suggests that the volcanism began in approximately 191 Ma (Sinemurian age) and continued until approximately 164 Ma, with at least three periods of increased volcanic activity. The inherited zircons contain Triassic, Permian, Neoproterozoic and Mesoproterozoic populations, indicating that this arc was emplaced on rocks of the Chibcha Terrane along the South American paleomargin and that it is part of the same arc that formed the Jurassic volcanic rocks of the Sierra Nevada de Santa Marta, Cocinas and San Lucas mountain ranges and the Upper Magdalena Valley.

Keywords: Jurassic; U-Pb geochronology; volcanic rocks; Perijá mountain range.

Resumen

Este trabajo presenta nuevos resultados de petrografía, química de roca total y geocronología U-Pb en circón de rocas volcánicas de la Formación La Quinta que afloran en el flanco occidental de la serranía de Perijá, en los departamentos de Cesar y La Guajira. Las rocas volcánicas corresponden a lavas basálticas, andesíticas, dacíticas y riolíticas, y las rocas volcanoclásticas corresponden a tobas cristalo-vítreas, cristalo-líticas y aglomerados de afinidad calcoalcalina, formadas en un ambiente de arco de margen continental. Los datos geocronológicos sugieren que el vulcanismo de la Formación La Quinta estuvo activo aproximadamente 25 Ma, intervalo en el que varió su composición de traquiandesitas basálticas a riolitas. Las edades U-Pb obtenidas sugieren que el vulcanismo se inició aproximadamente a 191

Ma (Sinemuriense) y se extendió hasta aproximadamente 164 Ma, con al menos tres periodos de mayor actividad volcánica. Los circones heredados presentan poblaciones del Triásico, Pérmico, Neoproterozoico y Mesoproterozoico, lo que sugiere que este arco se emplazó en rocas del Terreno Chibcha a lo largo de la paleomargen Suramericana y que son parte del mismo arco que formó las rocas volcánicas jurásicas de la Sierra Nevada de Santa Marta, la serranía de Cocinas, la serranía de San Lucas y el valle superior del Magdalena.

Palabras clave: Jurásico; geocronología U-Pb; rocas volcánicas; serranía de Perijá.

1. Introduction

The volcanic rocks of the La Quinta Formation outcrop at the northern end of the Colombian Cordillera Oriental [Eastern Ranges] in the Perijá mountain range, and they are part of the Jurassic volcanism that outcrops in the Upper Magdalena Valley in the San Lucas and Sierra Nevada de Santa Marta mountain ranges and in the Upper Guajira. The ages of these volcanic sequences range from 195 to 164 Ma (Cediel et al., 1980, 1981; Bustamante et al., 2010; Villagómez, 2010; Leal Mejía, 2011; Zapata et al., 2016; Rodríguez et al., 2018; Correa et al., 2019; Leal et al., 2019).

Most authors agree on the model of formation of the lower-to-middle Jurassic volcanism and plutonism of the northern Andes, which is considered to be continental margin arc magmatism. The following variations in the model and arc development have been proposed: 1) an arc formed by a single subduction zone located west of the South American margin, which was formed between 209 and 114 Ma (Spikings et al., 2015); 2) a stationary continental margin arc formed by oblique convergence between the Farallón plate (an ancient oceanic plate) and the NW of South America that has been active for at least 40 Ma (Bustamante et al., 2016); 3) a continental arc and back-arc comprising Jurassic rock blocks of the Upper Magdalena Valley, Colombian Cordillera Central [Central Andes], and San Lucas and Sierra Nevada de Santa Marta mountain ranges (Villagómez et al., 2015; Bayona et al., 2010); 4) an erosive continental margin arc that was active for ~30 Ma exhibiting a compositional migration in a west-east direction (Rodríguez et al., 2018); and 5) a continental margin arc that fragmented and scattered along the paleomargin after its formation (Bayona et al., 2010; Villagómez et al., 2015; Zapata et al., 2016; Zuluaga et al., 2015).

This study reports new petrography (9), total rock chemistry (8) and U-Pb zircon geochronology (laser ablation inductively coupled plasma mass spectrometry (LA-ICP-MS)) (5) data, which, together with published geochronology data (González et al., 2015a; González et al., 2015b) and with total the rock chemistry of the La Quinta Formation, supplement the basic information on this unit and on the volcanism associated with the arc dated to the Lower-Middle Jurassic.

This new information is correlated with other volcano-sedimentary sequences that outcrop in Colombia, specifies the distribution of arc volcanism and, together with the analysis of the inherited zircons in volcanic rocks, improves our understanding of the basement distribution on which the arc is founded and of the geological evolution of the northern Andean volcanism during the Jurassic while furthering our knowledge of the Jurassic tectonic blocks that were scattered along the paleomargin and their distribution, according to Bayona et al. (2010), Villagómez et al. (2015), Zapata et al. (2016) and Zuluaga et al. (2015).

2. Regional Geological Framework

The Perijá mountain range, which is located in the northern Cordillera Oriental [Eastern Ranges], uplifts from the Cerrejón and Yaya faults on its western edge, culminating in the Oca fault northward and forming a block bordered to the west by the Cesar-Rancherías river valley, which is a drainage basin filled with Mesozoic and Cenozoic sediments covered by recent alluvial deposits that separates the Perijá mountain range from the Sierra Nevada de Santa Marta block; to the north, the Oca fault separates the basin from the Cocinas mountain range in Upper Guajira (Figure 1).

The core of the Perijá mountain range consists of Precambrian gneissic metamorphic rocks, such as those observed in the Cachirí river, on the eastern slope of the mountainous range; the Río Cachirí Group rests on this gneiss basement (Pastor Chacón et al., 2013), although the gneiss basement has not been found on the western slope of the Perijá mountain range (Miller, 1960 and Forero, 1970). In the northern sector, the Perijá mountain range is essentially composed of Jurassic and Cretaceous units that cover Paleozoic units. The oldest rocks are Cambro-Ordovician metamorphic rocks and Devonian, Carboniferous and Permian sedimentary rocks (Forero, 1970; Pastor Chacón et al., 2013). On the western slope, the oldest unit of the Perijá mountain range contains Devonian sedimentites consisting of argillites, sandstone siltstones and limestones (Weisbord, 1926; Trumpy, 1943; Miller, 1960; Forero, 1970 and Pastor Chacón et al., 2013).

The Jurassic volcano-sedimentary sequences of the La Quinta Formation rest on Paleozoic outcrops of the western slope of the Perijá mountain range. These sequences consist of red beds of sandstones, siltstones, argillites, conglomerates, subordinate lavas and subaerial pyroclastic rocks, where the former are similar to those exposed on the eastern slope of Sierra Nevada de Santa Marta, where abundant Jurassic volcanic rocks outcrop (Tschanz et al., 1969).

Cretaceous sedimentary sequences appear on both banks of the Cesar-Rancherías valley (Molino Formation, Cogollo Group and La Luna and Portales formations). These sequences rest on the La Quinta Formation and Jurassic Vulcanites of the Sierra Nevada de Santa Marta (SNSM). Similarly, Paleocene-to-Miocene sedimentary sequences, such as the Cerrejón Formation, rest on the Cretaceous units.

3. History of La Quinta Formation

The La Quinta Formation consists of red sediments that stratigraphically lie above Paleozoic units and below Mesozoic units. This unit was described by Kundig (1938) in the state of Táchira on the Seboruco-La Grita road near the La Quinta hamlet in Venezuela. The sequence, towards the base, is made up of compact dark red conglomerates with well-cemented rims and with sandstone and red clay intercalations.

In Colombia, Miller (1960) coined the term *La Quinta Formation* to refer to the likely Jurassic sediments that are found on the western slope of the Perijá mountain range, on the western slope of the Ranchería and Cesar rivers, and on the Majuyura Ridge (Oca fault) at the northern end of the Perijá mountain range.

Radelli (1962) continues using the term *La Quinta Formation* coined by Miller (1960), considering the stratigraphic correspondence with the La Quinta Formation of the Venezuelan authors, the sedimentation environment and the presence of volcanic material. Radelli (1962) describes the sequence as a predominantly detrital succession, albeit noting the presence of volcanic material. This author distinguishes the following facies: a) conglomerates with volcanic pebbles, which form the basement; b) acidic volcanic rocks associated with sandstones; and c) the fine-grained red sandstones that make up most of the La Quinta Formation, with interbedded tuffs and with sandstones at the basement of the formation, together with andesitic lavas, where there are conformities and unconformities between the sediments described above.

Forero (1972) surveyed a stratigraphic column of the La Quinta Formation in Manaure, Cesar Department (Colombia), and identified the following five sets of rocks from bottom to top: a) conglomerates, red sandstones and volcanic rocks; b) red sandstones and lutites; c) red sandstones with tuff intercalations; d) conglomerate with volcanic pebbles; and e) rhyolitic tuffs.

Hernández (2003) describes the sequence of the La Quinta Formation in the Perijá mountain range east of the towns of La Jagua de Ibirico in the sector of La Victoria de San Isidro and southeast of Santa Isabel, which shows a succession along the western flank of the mountain range. Arias and Morales (1999) report that this unit outcrops near the municipality of Manaure and continues south to the San Antonio gorge, with a thickness ranging from 2,700 to 3,000 m, whereas its thickness markedly decreases in La Jagua de Ibirico due to local reverse faults that affected the unit through tectonic uplift in the Miocene during the Andean orogeny.

Geoestudios (2006) describes the La Quinta Formation as a sequence consisting of purple-red, aphanitic ash tuffs and welded ash-flow tuffs with pseudolamination, together with slightly calcareous mudstones, conglomerate sandstones and matrix-supported conglomerates,

with local interbedding of reddish mudstones and arkosic sandstones with cross-bedding.

González et al. (2015 a and b) describe volcanic and pyroclastic rocks throughout the sequence of the La Quinta Formation, consisting of basalts, andesites, dacites, rhyolites and calc-alkaline subalkaline pyroclastic rocks, formed in a continental volcanic arc setting and with Lower to Middle Jurassic U-Pb ages.

3. Methodology

Regional sampling was performed from the volcanic rocks of the La Quinta Formation in the Perijá mountain range and the Cesar and La Guajira departments for this study. In this sampling, sixteen rocks were taken, with eleven additional samples for zircon extraction; fifteen new thin sections were prepared, total rock chemical analysis was performed on eight rocks, and six samples were dated by zircon U-Pb LA-ICP-MS.

3.1 Petrography

Initially, petrographic analyses were performed from the mapping projects of the Servicio Geológico Colombiano; previously known as Ingeominas. In the present study, rock samples were selected for petrography from a larger number of samples collected in field work. The selection criteria used in this study were undisturbed rocks with defined spatial distribution representative of the volcanic rocks that make up the La Quinta Formation. Fifteen new samples were sent to the Thin Section Preparation Laboratory of the Servicio Geológico Colombiano, Bogotá headquarters. Once the thin sections were prepared, they were analyzed by the authors at the Petrography Laboratory of the Servicio Geológico Colombiano in Medellín, using SGC standards in the analysis with Leitz and Olympus petrographic microscopes and classifying the samples from 300 counting points, according to the quartz, alkali feldspar, plagioclase, feldspathoid (QAPF) diagrams by Streckeisen et al. (1978) and following the recommendations of Le Maitre et al. (2002).

3.2 Total rock chemical analysis

Eight fresh rocks were chosen, taking into account the previous petrographic analysis, which was followed by total rock chemical analysis at the Analytical Geochemistry Laboratory of the Servicio Geológico Colombiano, Bogotá headquarters. The major oxides and minor elements were analyzed with a Panalytical Axios Mineral X-ray fluorescence spectrometer; the major oxides were quantified using samples fused with lithium metaborate and lithium tetraborate, whereas the minor elements were quantified using pressed samples. The trace elements were analyzed using a Perkin Elmer Nexion inductively coupled plasma mass spectrometer (ICP-MS). The findings of González et al. (2015 a, b) were compared with the results from the present study since both were based on samples collected from the same region.
Petrographic and geochemical diagrams were prepared using the GCDkit software by Janoušek et al. (2006).

3.3 U-Pb geochronology

Eleven samples were chosen for zircon separation after petrographic and chemical analysis of the total rock. Of these samples, from only six samples of lava and pyroclastic volcanic rocks, enough zircons were obtained for LA-ICP-MS U-Pb zircon dating. The rock samples were crushed, pulverized and sieved following the separation procedure of Castaño et al. (2018) and analyzed by LA-ICP-MS according to the procedure described by Peña et al. (2018). Most zircons were concentrated at the Chemistry Laboratory of Geological Surveys, Medellín headquarters, using hydrodynamic and magnetic separation and others were concentrated in the field using a gold pan. The zircons were selected manually using an Olympus stereo microscope at the Petrography Laboratory, Medellín headquarters. Cathodoluminescence (CL) images of the zircon grain mounts were acquired under a Zeiss scanning electron microscope (SEM) with a GatCL miniCL detector to observe the internal structure of the selected grains.

The analyses were performed in a Photon Machines laser ablation system with a 193-nm excimer laser coupled to an Element 2 mass spectrometer. The isotopes used for manual integration were ^{238}U, ^{206}Pb and ^{204}Pb. Plešovice zircon (Sláma et al., 2008), FC-1 (Coyner et al., 2004), Zircon 91500 (Wiedenbeck et al., 1995; Wiedenbeck et al., 2004) and Mount Dromedary (Renne et al., 1998) were used as reference standards. The points analyzed in the zircons were 20 microns in diameter. Data reduction was performed using the Iolite v2.5® software

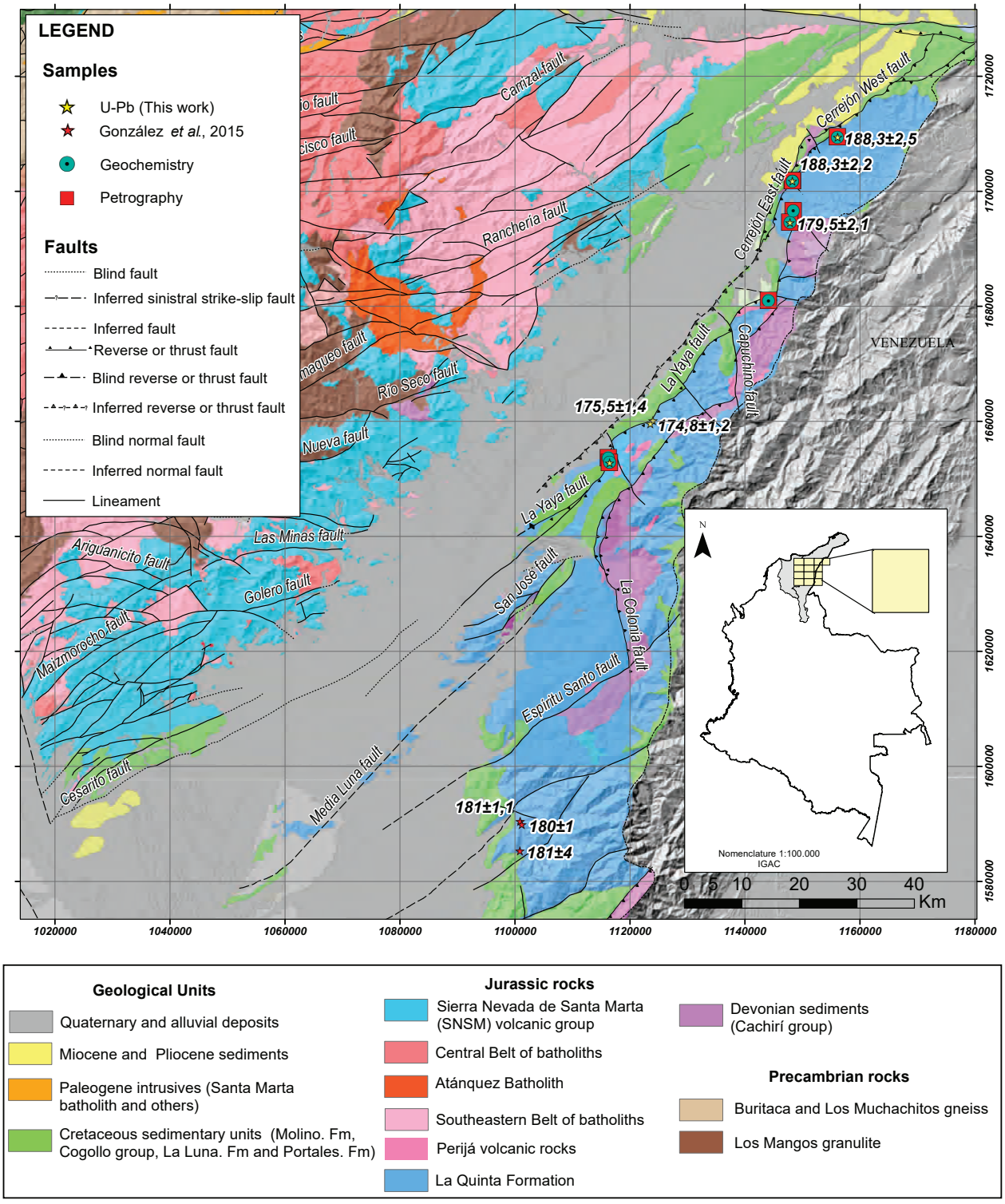

Geological Units

- Quaternary and alluvial deposits
- Miocene and Pliocene sediments
- Paleogene intrusives (Santa Marta batholith and others)
- Cretaceous sedimentary units (Molino. Fm, Cogollo group, La Luna. Fm and Portales. Fm)

Jurassic rocks

- Sierra Nevada de Santa Marta (SNSM) volcanic group
- Central Belt of batholiths
- Atánquez Batholith
- Southeastern Belt of batholiths
- Perijá volcanic rocks
- La Quinta Formation

- Devonian sediments (Cachirí group)

Precambrian rocks

- Buritaca and Los Muchachitos gneiss
- Los Mangos granulite

Figure 1. Geological map of the La Quinta Formation. Distribution of samples with thin sections, lithogeochemistry and geochronology with U-Pb dating
Source: González et al. (2015 a, b); Invemar et al. (2007)

in IGORPro 6.3.6.4® (Paton et al., 2010; Hellstrom et al., 2008). Common lead correction was performed using the evolution model according to Stacey and Kramers (1975). The final results corresponded to the mean of the data that fell within two standard deviations.

The ages were determined by the youngest results in each sample (assuming that this group of zircons crystallized during the same magmatic episode) because this provides the best estimate of the rapid crystallization of pyroclastic or volcanic material. The analysis was performed sample by sample when the youngest data corresponded to one or more populations by considering probability density plots and zircon by zircon when more than one population was identified by analyzing the ablation sites and the internal structure of each zircon, initially separating the ablations into cores and rims and then grouping them. This method was used to separate the populations of xenocrystals and inherited zircon cores. In the populations that defined the crystallization age and suggested the presence of antecrystals, the zircons were compared. Whether the ablation sites corresponded to cores or rims was analyzed, and the age of the entire population was calculated, which could define the crystallization age; additionally, the weighted average age of the antecrystals and the weighted average age of the younger zircons was calculated, which likely defined the crystallization age of the rock. The findings were compared with the crystallization episodes of the arc in both the plutonic and volcanic rocks (Rodríguez et al., 2018; Rodríguez et al., 2019b; Correa et al., 2019).

The $^{207}Pb/^{206}Pb$ ratios, ages and errors were calculated according to Petrus and Kamber (2012). The concentrations of U and Th were calculated according to Paton et al. (2010) using an external standard zircon. The ages and the geochronology plots were calculated and drawn, respectively, using the add-in program Isoplot v4.15 (Ludwig, 2012). The graphical representation in the article is a single weighted average age diagram showing the zircons that indicate the age of the crystals and the age of crystallization, albeit with the age calculated separately in the program.

4. Results

4.2 Petrography

The La Quinta Formation, located in the Perijá mountain range and the Cesar and La Guajira departments, primarily consists of conglomerates, conglomeratic sandstones and reddish and subordinately brown, gray and greenish gray sandstones, usually in thick-to-very-thick wavy layers, some of which include cross-bedding.

Less frequently, violet rhyolitic, dacitic, andesitic and basaltic lavas are identified, as well as thick interbedded layers of crystal-vitric and crystal-lithic tuffs and agglomerates with ash matrix and lapilli. The volcanic rocks of this study are violet. The petrographic results are summarized in Figure 2 and Table 1.

Basalts. The basalts have a fluid trachytic, porphyritic texture, and some of the basalts show irregular zeolite-filled amygdules, epidote and epidote and quartz. The

Table 1. Modal classifications in percentages for volcanic rocks of the La Quinta Formation

IGM	W	N	Qz	Pl	Fsp	Cpx	Ol	Hbl	Bt	Op	Ap	Zrn	Ep	Matrix	FR	Other	Classification
901373	1124017	1660152	16	12.1	10			1.5		1.9		0.4	0.8	29.2		30	Vitreous tuff
901609	1148285	1701812	3.6	15.8	0.8	7.1				2	0.8			69.9			Dacite
901377	1148433	1696644	1.4	21	0.7	1	tr			1				71.9		3	Andesite
901631	1123566	1659592	33	20.8						2.1			2.1	41.7			Dacite
901624	1156113	1709417		22.5				5.3		8.6	tr			63.6			Phenoandesite
901625	1116457	1652853		57.6			1			1.3				40.1			Basalt
901382	1116236	1653658		45.6			16.2			38.2							Olivine basalt
901437	1144105	1681005	0.1	79.9		8.4				11.6			3.1				Trachytic basalt
901623	1147831	1694625	1.2	8.4	2.1			0.5	0.6	2.4	Tr	Tr		32.4	50.6	1.8	Lithic tuff

Qz: quartz, Pl: plagioclase, Fsp: feldspar, Cpx: clinopyroxene, Ol: olivine, Hbl: hornblende, Bt: biotite, Op: opaque minerals, Ap: apatite, Zrn: zircon, Ep: epidote, FR: lithic fragments, tr: traces. Coordinates in Magna Sirgas, Bogotá

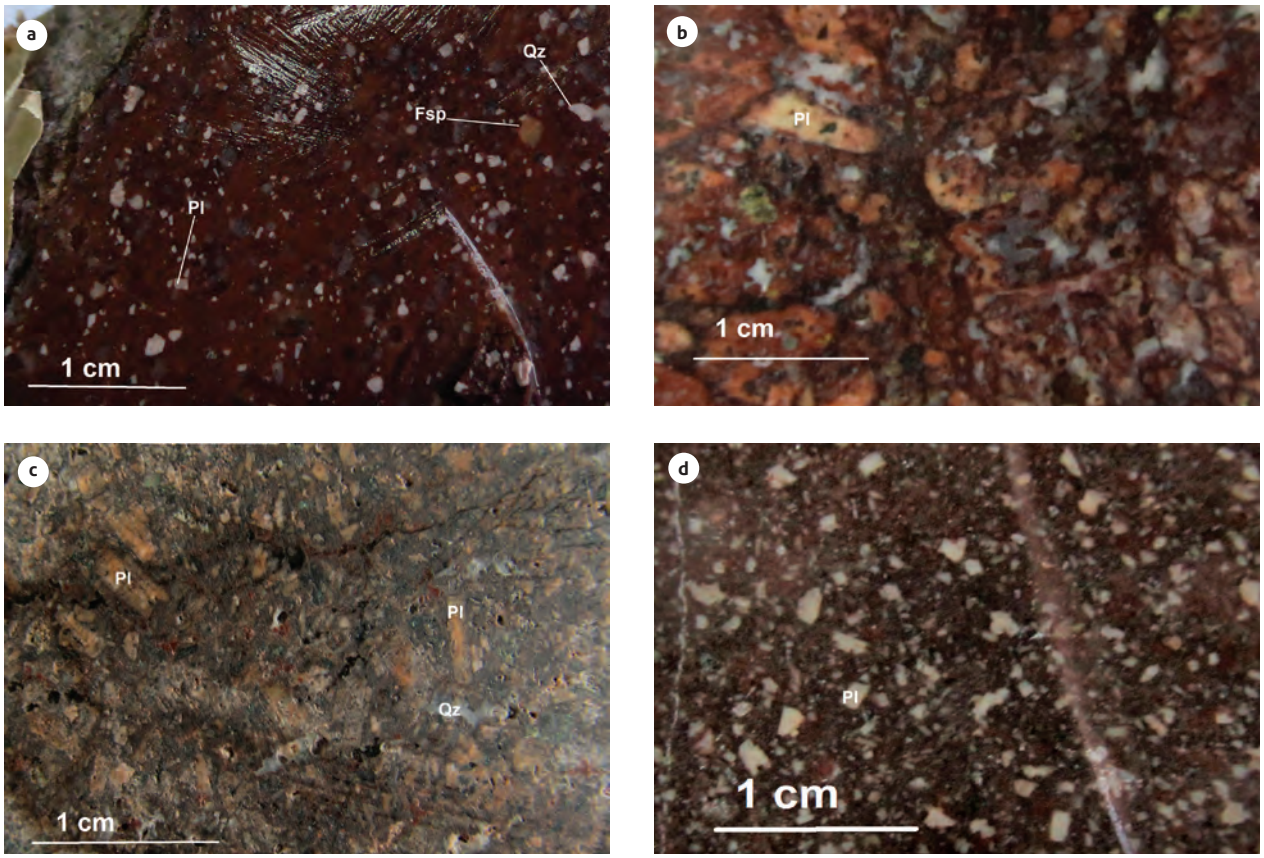

Figure 2. Macroscopic observations of lavas and tuffs of the La Quinta Formation
A) 901373-Tuff. B) 901377-Tuff. C) 901609-Dacite. E) 901624-Phenoandesite

phenocrysts are mainly skeletal olivine (0.1-16%) inside a trachytic matrix consisting of tabular plagioclase euhedral microcrystals (45.6%-79.9%), glass and intersertal opaque minerals (hematite 1.3%-11%), and some of the rocks contain clinopyroxene (0%-8.4%). The skeletal olivine phenocrysts are euhedral to subhedral, with sizes ranging from 700 μn to 3 mm and with irregular fractures marked by opaque minerals altered to hematite, and are completely replaced by serpentine and epidote inside the crystals. The accessory minerals are microcrystals of opaque minerals (hematite). The alteration minerals are serpentine and epidote from olivine; the plagioclase can be dusted due to an alteration to saussurite, and the glass, in some rocks, is altered to epidote and sericite (Figure 3A and B).

Rhyolites and dacites. Rhyolites and dacites are rocks with microporphyritic, porphyritic and sometimes seriate textures. These rocks consist of euhedral microphenocrysts to phenocrysts of quartz (6.6%-38%), plagioclase (12%-45%), sanidine (0%-10%) and may contain hornblende. The phenocrysts are dispersed in a matrix ranging from hyalocrystalline to fluidal microlithic; the matrix can be devitrified and altered to secondary sericite and epidote aggregates. The accessory rocks are ochre hematite, which accounts for the color of the rocks, apatite and zircon. The quartz can be euhedral-to-subhedral bipyramidal, with matrix corrosion bays and uneven internal matrix droplets. The plagioclase ranges from 3 to 0.1 mm and is found in euhedral crystals, with zonation. The alteration minerals are sericite and clay in plagioclase and feldspar and chlorite in amphiboles.

Pyroclastic rocks. The rocks correspond to red-to-violet, and less frequently greenish-gray, tuffs and volcanic agglomerates and consist of lithic fragments of crystals and altered glass.

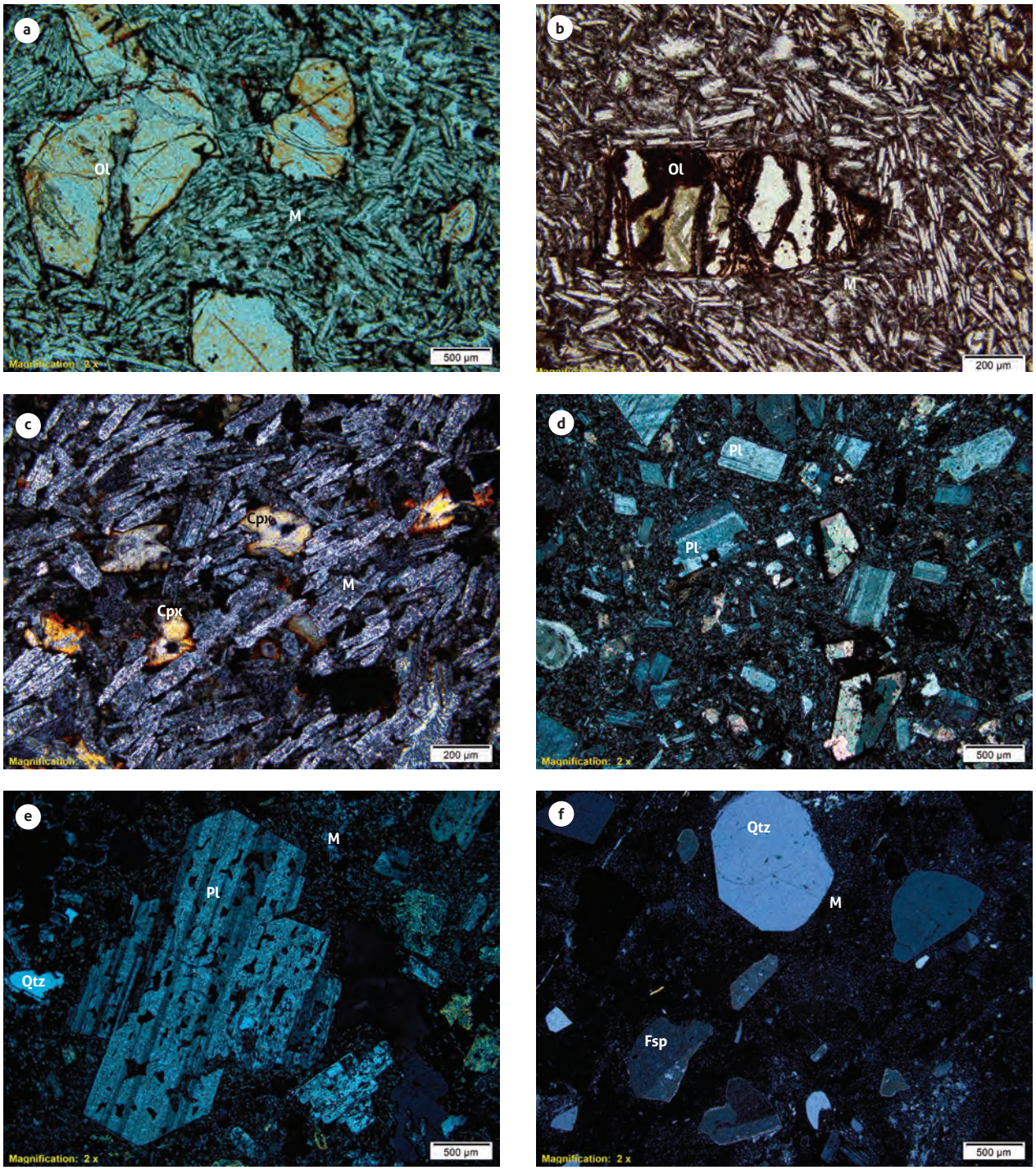

Figure 3. Microscopic observations of lavas and tuffs of the La Quinta Formation
A, B) Samples IGM 901382 and IGM 901625: basalts consisting of skeletal olivine (Ol) phenocrysts suspended in a trachytic plagioclase matrix (M). C) Sample IGM-901437: basaltic andesite with clinopyroxene (Cpx) phenocrysts suspended in a trachytic plagioclase matrix (M). D) Sample IGM 901624: andesite, seriate plagioclase (Pl) phenocrysts and skeletal hornblende (Hbl) suspended in a vitreous matrix (M). E) Sample IGM 901609: andesite with plagioclase (Pl) phenocrysts and quartz in a microlithic matrix (M). F) Sample IGM 901373: crystalline vitreous tuff with quartz (Qtz) and feldspar (Fsp) crystals suspended in a vitreous matrix (M)

The tuffs consist of volcanic lithic fragments of andesites and basalts with porphyritic textures and vitreous, trachytic, fluidal microlithic and devitrified matrix, with plagioclase phenocrysts and, less frequently, with skeletal mafic minerals replaced by opaque minerals and epidote, with sizes ranging from 300 microns to 6 mm (ash and lapilli). The suspended and scattered fragments range from angled and rounded to amorphous. Some crystal fragments of quartz, plagioclase, sanidine, hornblende and biotite range from 0.2 to 1.8 mm. The crystals and crystal fragments are anhedral to euhedral. The quartz can be bipyramidal and have corroded rims, with corrosion bays and paste or devitrified glass inclusions. The plagioclase and sanidine crystals are tabular euhedral and are covered with their alteration to kaolin; the hornblende and the biotite usually occur as skeletal crystals completely replaced by opaque minerals. The matrix consists of devitrified glass and fragments of quartz crystals and feldspars smaller than 80 microns, with widespread apatite, zircon and opaque minerals as accessory minerals (Figure 3F).

5. Geochemistry

Eight samples of lavas, agglomerates and tuffs were analyzed. The spatial distribution of the samples is shown in Figure 1. The contents of the major oxides and trace and rare-earth elements (REE) are presented in Tables 2 and 3.

The samples IGM 901610, IGM 901382 and IGM 901624 present 3.41%. 3.60% and 4.30% losses on ignition (LOIs), respectively. The sample IGM 901382, classified as basalt, shows olivine phenocrysts that are completely altered to serpentine; the sample IGM 901624, classified as andesite, shows skeletal hornblende that is altered to calcite and calcite veinlets, and the sample IGM 901377, classified as andesite, presents hydrothermal quartz veins. The analysis of the possible rock alterations from the diagram of Hughes (1972) demonstrated that the samples IGM 901624, IGM 901623, IGM 901610 and IGM 901377 show sodic alteration (Figure 4).

Table 2. Results for major oxides in lavas and pyroclastic rocks of the La Quinta Formation

IGM	901609	901610	901377	901382	901437	901623	901624	901625
Field No.	GOE-1045A	GOE-1045B	GOE-1048	GOE-1058	GR-6821	GR-6849	GR-6851	GR-6854
W	1148285	1148285	1148433	1116236	1144105	1147831	1156113	1116457
N	1701812	1701812	1696644	1653658	1681005	1694625	1709417	1652853
SiO2	60.57	59.55	58.24	51.27	51.29	70.43	55.66	57.75
TiO2	1.05	0.87	1.20	1.36	1.49	0.48	1.21	1.08
Al2O3	17.35	16.05	15.28	15.32	15.45	14.39	18.31	15.16
Fe2O3T	6.09	6.60	7.80	8.70	9.08	3.08	5.41	7.30
MgO	1.83	4.66	2.27	7.32	6.64	1.01	2.64	4.57
CaO	1.16	1.29	5.60	5.11	5.83	1.03	3.50	3.47
Na2O	6.19	5.59	5.30	4.38	4.53	6.23	7.53	5.21
K2O	3.42	1.49	1.10	2.24	1.82	1.84	0.81	2.64
P2O5	0.247	0.292	0.465	0.345	0.526	0.146	0.298	0.325
MnO	0.01	0.01	0.01	0.02	0.02	0.00	0.01	0.01
LOI	1.88	3.41	2.53	3.60	2.99	1.27	4.30	2.19

The SiO_2 values of lavas and pyroclastic rocks range from 51.3% to 70.4%, and the Fe_2O_3, MgO and CaO values decrease with increasing SiO_2 (Table 2); the Na_2O values increase with increasing SiO_2, and the K_2O content is variable and dispersed. The TiO_2 values are higher and lower than 1%, with most values > 1%, except for samples GOE-1045B and IGM- 901623 (GR-6849), with TiO_2 < 1%. The Al_2O_3 content ranges from 14.4% to 18.3%; Fe_2O_3 ranges from 3.1% to 9.1%; MgO ranges from 1 to 7.3%; CaO ranges from 1% to 5.8%; the alkali ($Na_2O + K_2O$) content is high, ranging from 6.3% to 9.6%, with K_2O/Na_2O ratios < 0.6%

Table 3. Results for trace elements of volcanic rocks of the La Quinta Formation

IGM	901382	901437	901609	901610	901624	901625	901377	901623
Field No.	GOE-1058	GR-6821	GOE-1045A	GOE-1045B	GR-6851	GR-6854	GOE-1048	GR-6849
Chemical classification	Basaltic trachyandesite	Basaltic trachyandesite	Trachydacite	Trachyandesite	Trachyandesite	Trachyandesite	Trachyandesite	Rhyolite
W	1116236	1144105	1148285	1148285	1156113	1116457	1148433	1147831
N	1653658	1681005	1701812	1701812	1709417	1652853	1696644	1694625
Y	27	25	24	26	27	21	22	18
Li	33.5	65.7	23.12	53.37	31.19	27.60	13.7	10.31
Be	1.70	2.01	1.77	2.37	1.57	1.38	1.79	2.07
Sc	24.82	21.60	20.7	20.5	22.0	21.5	17.78	5.8
Co	40.8	41.6					27.5	
Ga	17.3	18.3	21	34	20	18	17.9	20
As	2.82	9.14	4.5	5.2	4.7	2.5	3.88	4.7
In	0.06	0.08	0.05	0.06	0.05	0.06	0.05	0.03
Cs	0.29	0.22	0.80	1.35	0.62	1.12	0.38	0.13
Ba	618	829	1972	352	181	1359	442	241
La	23.6	30.0	40	24	36	30	28.3	112
Ce	55.7	75.1	88	68	76	71	69.9	119
Pr	7.6	11.6	10.6	8.8	9.4	8.5	9.6	14.2
Nd	27.1	46.2	13.0	18.4	14.1	11.7	35.9	5.1
Sm	6.7	9.4	7.12	7.03	6.79	6.70	7.7	6.77
Eu	2.0	2.8	2.01	1.85	1.21	2.03	2.1	1.58
Gd	6.3	7.9	6.48	6.39	6.41	6.14	6.9	6.64
Tb	0.92	1.16	0.85	0.88	0.90	0.89	0.89	0.77
Dy	4.94	5.90	3.93	4.73	4.77	4.63	4.48	3.58
Ho	1.01	1.14	0.73	0.87	0.90	0.87	0.83	0.67
Er	2.80	3.18	2.01	2.59	2.57	2.48	2.29	1.93
Tm	0.38	0.40	0.25	0.34	0.34	0.33	0.30	0.25
Yb	2.34	2.60	1.59	2.17	2.10	2.09	1.92	1.61
Lu	0.33	0.38	0.23	0.33	0.31	0.31	0.25	0.23
Tl	0.34	0.46	0.41	0.22	0.10	0.38	0.18	0.26
Pb	6.1	8.0	15.4	7.9	13.7	6.2	9.1	7.2
Th	2.83	2.82	4.94	3.48	4.65	4.51	3.82	10.18
U	0.73	0.62	1.15	0.67	1.09	1.27	1.05	1.51
Nb	12	14	8	7	9	11	13	8
V	< 66	123	131	125	148	167	101	74
Rb	56	44	63	58	16	153	23	41
Sr	439	518	261	232	483	406	335	186

In the total alkali–silica (TAS) diagram (Le Bas et al., 1986), the lava and pyroclastic rocks are located in the fields of basaltic trachyandesites, trachyandesites, trachydacites and rhyolites, with wide compositional variation

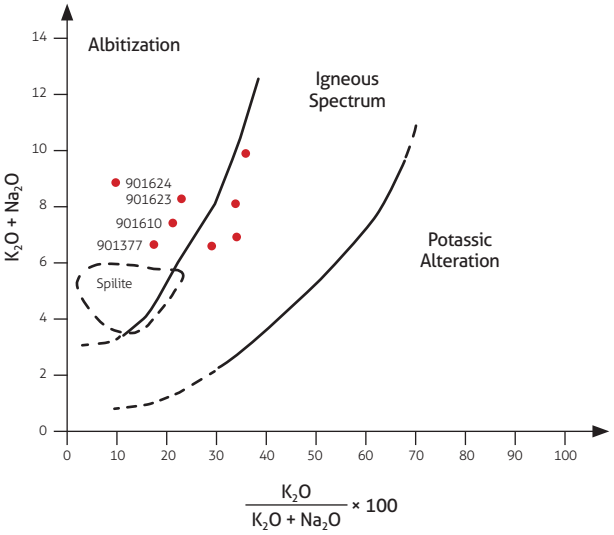

Figure 4. Samples of the La Quinta Formation for identifying alteration according to the diagram of Hughes (1972)

(Figure 5A). The samples IGM 901382, IGM 901437, IGM 901624, IGM 901625 and IGM 901609 are classified in the alkaline series, and the samples IGM 901625, IGM 901377 and IGM 901623 are classified in the subalkaline series. The TAS diagram is similar to that obtained in the model classification of the rocks in the diagram of Streckeisen (1978). In the Nb/Y vs. Zr/Ti diagram (Winchester and Floyd, 1977), the samples of lavas and pyroclastic rocks primarily correspond to the fields of andesites and subalkaline rhyodacites (Figure 5B). The rocks of the La Quinta Formation are metaluminous, and some reach the field of peraluminous rocks (IGM 901609, IGM 901610, IGM 901623), with A/CNK values ranging from 0.7 to 1.3. The A/NK values range from 1 to 2 (Figure 5C). The rocks show a wide dispersion in the SiO_2 vs. K_2O diagram and are distributed in the fields of normal-to-high-K calc-alkaline rocks (Figure 5D).

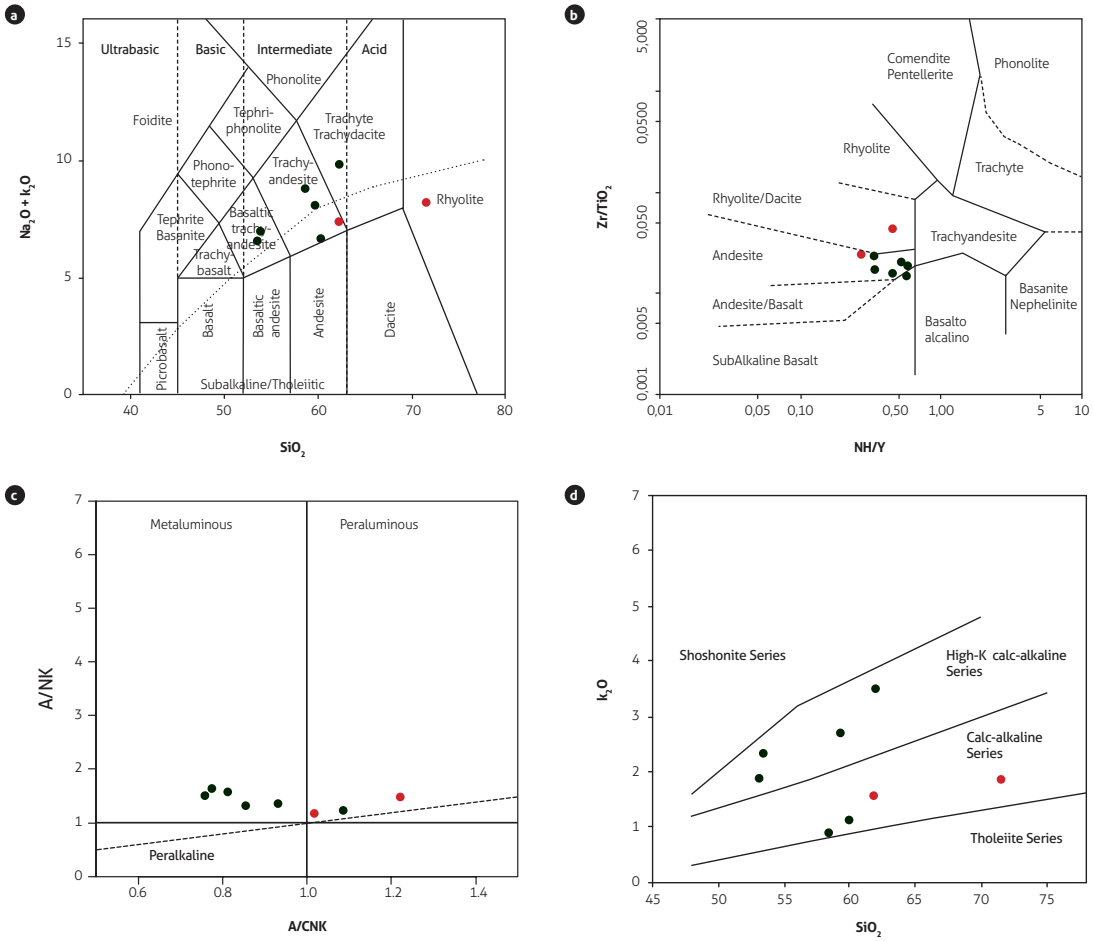

Figure 5. Classification diagram of volcanic rocks of the La Quinta Formation; lavas in black and tuffs in red
A) TAS diagram (Le Bas et al., 1986). B) Winchester and Floyd (1977) classification diagram. C) Shand classification diagram. D) SiO_2 vs. K_2O diagram (Peccerillo and Taylor, 1976)

5.1 Trace elements

The behavior of these elements is analyzed considering the SiO_2 content of the rocks and the chemical classification to determine whether there are relationships between the patterns of rare-earth elements (REE), trace elements and SiO_2 content.

The chondrite-normalized (Nakamura, 1974) REE diagrams of basaltic trachyandesites show a parallel pattern, with a negative slope and with a light-REE enrichment of 70 to 100 times. The $(La/Yb)_N$ ratio ranges from 6.7 to 7.8 and has no Eu anomalies, and the Eu/Eu* ratio is approximately 1. The patterns of trachyandesites and trachydacites are subparallel, and these rocks are slightly more depleted of Tm, Yb and Lu than basaltic trachyandesites. The Eu anomaly ranges from 0.56 to 0.97, and the $(La/Yb)_N$ ratio ranges from 7.3 to 16.8. The rhyolitic tuff has a pattern with an even more negative slope and higher light-REE enrichment, between 300 and 400 times, and further heavy-REE depletion, with Eu and Ce anomalies, indicating plagioclase fractionation and possible contribution of sedimentary material to the source. In the rhyolitic tuff, the Eu/Eu* ratio is 0.7, and the $(La/Yb)_N$ ratio is 46.6 (Figure 6A, C and E). The higher values of the $(La/Yb)_N$ ratio in rhyolite could represent greater contributions from the crust and periods of higher magma flux and/or thicker crust. Lower values of the $(La/Yb)_N$ ratio could indicate greater contributions of mantle materials to the magma and periods of lower magmatic flux (Girardi et al., 2008).

The lavas of the La Quinta Formation, in the normal mid-ocean ridge basalt (NMORB)-normalized trace element diagram (Sun and McDonough, 1989), show negative Nb and Ti anomalies and positive anomalies and high values of Cs, Rb, Ba, Th, K and Pb, which suggests affinity with the continental crust (convergent margins), where these highly incompatible elements abound. The high values of Ba and Rb may result from their mobilization from fluids that interact with magma in the subduction zone. All of these features are characteristic of magmas generated in arc settings (Pearce et al., 1984; Pearce, 1996), with gradual depletion of large-ion lithophile elements (LILE) and enrichment in high-field-strength elements (HFSE; Figure 6). The basaltic trachyandesitic, trachyandesitic and dacitic lavas show similar multielement patterns, with higher Cs, Rb and Ba mobility in trachyandesites and with negative Nb and Ti and positive K and Pb anomalies. The andesitic pyroclastic rocks have multielement patterns in trace elements similar to those of lavas, suggesting that they are cogenetic (Figure 6B and D). The sample of rhyolitic tuff shows a different pattern, with more pronounced negative Nb, P and Ti anomalies (Figure 6F), suggesting at least three magmatic events, as proposed by Cano et al. (2017).

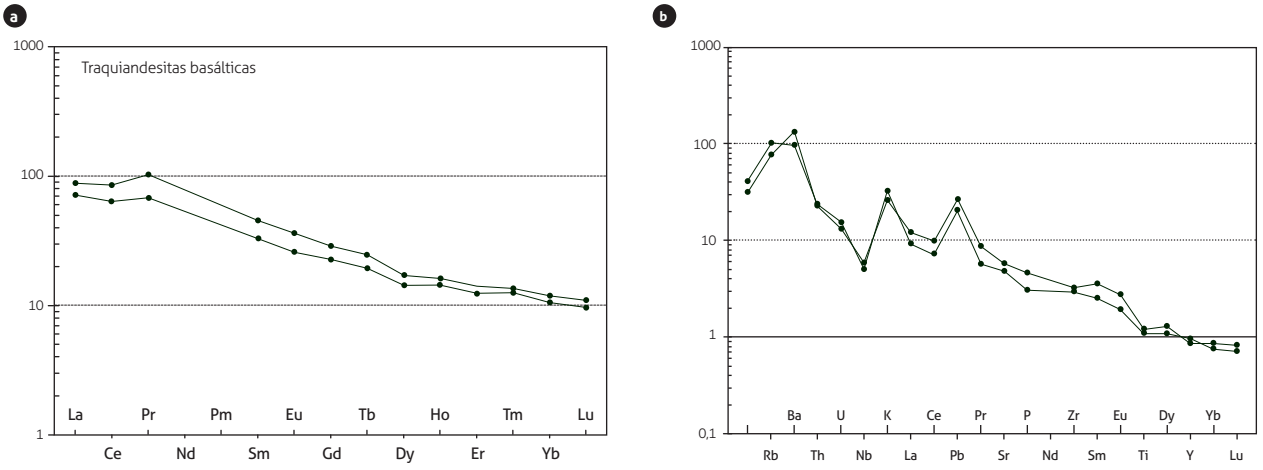

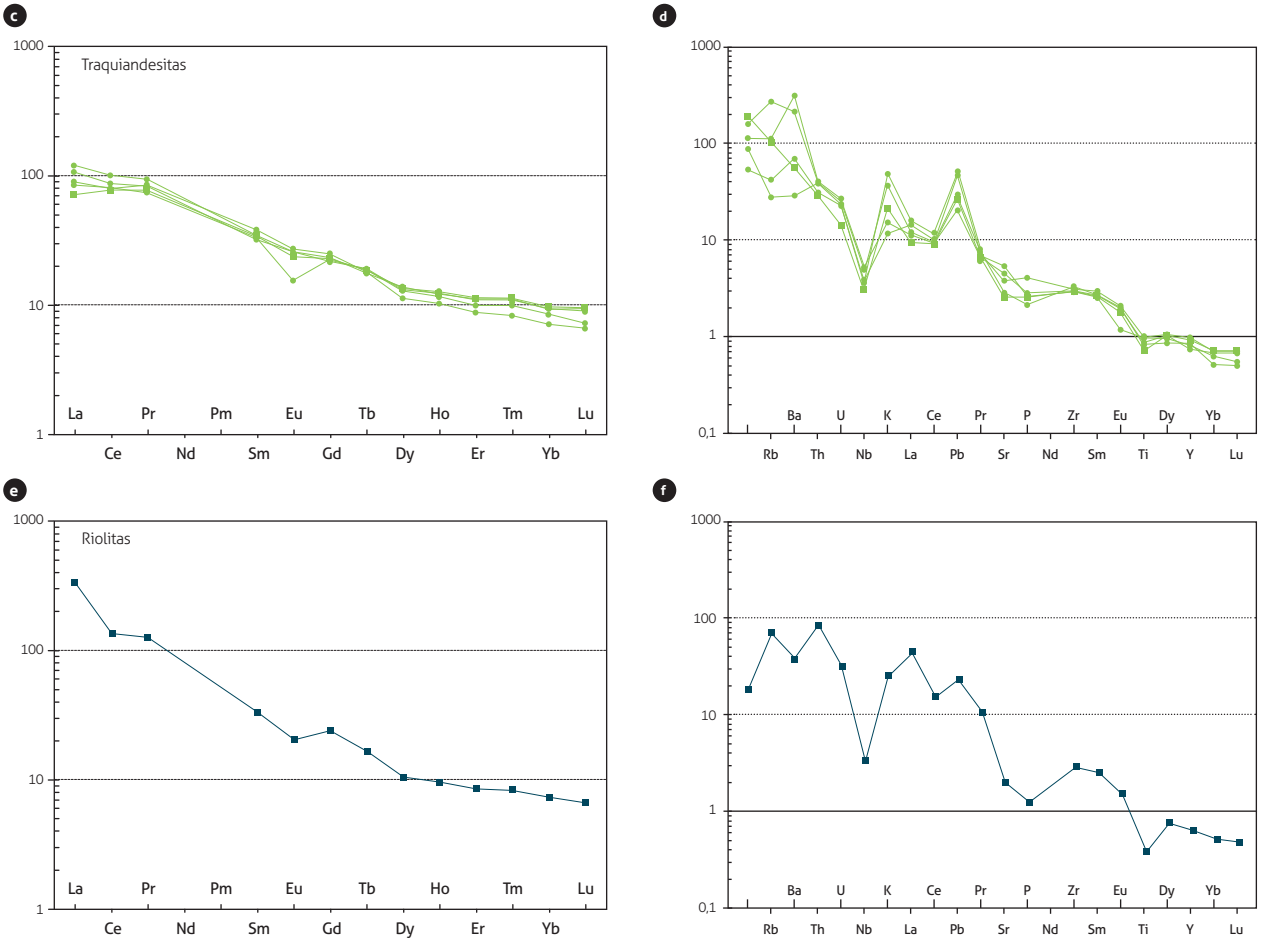

Figure 6. Multielement diagrams corresponding to volcanic and pyroclastic rocks of the La Quinta Formation
A, C, E) Chondrite-normalized REE diagrams (Nakamura, 1974). B, D, F) NMORB-normalized multielement diagrams (Sun and McDonough, 1989)

5.2 Tectonic setting discrimination

The presence of basaltic trachyandesites, trachyandesites, dacites and calc-alkaline rhyolites, together with Nb and Ti anomalies in the multielement diagrams and negative slopes in the REE diagrams, suggests that the volcanic rocks of the La Quinta Formation were generated in an arc setting. The lavas and pyroclastic rocks of the La Quinta Formation, in the Sr/Y vs $(La/Yb)_N$ diagram (Condie and Kröner, 2013), are plotted in the field of continental volcanic arcs, with enrichment in $(La/Yb)_N$ as the rocks become more differentiated (Figure 7). Basaltic trachyandesites, trachyandesites and rhyolites are grouped separately, and rhyolite is plotted outside the field, although in other diagrams, such as that of Pearce (2008), rhyolite falls within the field of arcs.

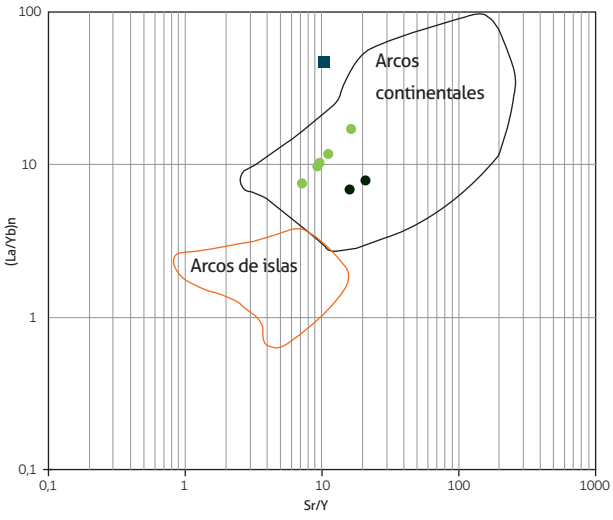

Figure 7. Nb/Yb vs Th/Yb diagram of Condie and Kröner (2013) for rock samples from the La Quinta Formation

6. Geochronology

For the geochronological analysis of the volcanic rocks of the La Quinta Formation, six rocks were analyzed using the U-Pb zircon LA-ICP-MS method. The U-Pb ages reported by González et al. (2015 a, b) were collected and are outlined in Table 4, and the corresponding spatial locations are shown in Figure 1. The reported ages are calculated with the Pb^{206}/U^{238} ratio. In general, all the ages show dispersion in each of the dated samples. This phenomenon is well-documented in igneous systems, due to the long crystallization of zircon within the magmatic system (Schoene et al., 2015) or to Pb loss and the presence of older inherited zircons in the magma (antecrystals). The crystallization age of each rock is calculated considering the presence or absence of populations of ages according to the probability density diagram and the observable distribution in the Tera-Wasserburg diagram, which could suggest populations of antecrystals. For this purpose, cathodoluminescence images and the age of each zircon are analyzed, as well as the locations of zircon ablations, for which the younger zircon populations are separated from the zircon populations of the magmatic system that could correspond to the ages of the antecrystals. Three ages are determined in the rocks that show high dispersion of ages according to the Pb^{206}/U^{238} ratio: the age of the entire population, the age of the likely antecrystals and the youngest age of likely crystallization. These ages are analyzed in the discussion.

Table 4. Summary of U-Pb ages determined by LA-ICP-MS in zircon samples of the La Quinta Formation

Sample No.	W Longitude	N Latitude	Rock	Age (Ma)	MSWD	Inheritances	Reference
GOE-1045a	1148285	1701812	Trachydacite	188.3 ± 2.2	3.9	1,902.2 ± 70 (n = 1); 1,138-1,191 (n = 2); 1,010.2-1,097 (n = 5); 856.2 ± 21.6 (n = 1); 931.1 ± 22 (n = 1); 613.5 ± 15; 210-218 (n = 3)	Present study
GR-6849	1147831	1694625	Tuff*	179.5 ± 2.1	4.3	1.974.3; 1,369-1.311 (n = 3); 1,283-1,209 (n = 3); 1,076-926.3 (n = 5); 992-926.3 (n = 4); 873.3-855.9; 623 ± 25.6; 556-551 (n = 3); 287.7 ± 8 (n = 1)	Present study
GR-6851	1156113	1709417	Trachyandesite	188.3 ± 2.5	6.6	1,913.8 ± 39.7 (n = 1); 1,361.1 ± 31 (n = 1), 892.6-996.2 (n = 2); 625.4-605.2 (n = 2); 226.2-203.5 (n = 4)	Present study
GOE-1057	1124017	1660152	Vitreous tuff*	175.5 ± 1.4	5.3	1,263.2 ± 33 (n = 1); 956.2-969.5 (n = 2).	Present study
GZ-6903	1123566	1659592	Dacite*	174.8 ± 1.2	3.4	1,515 ± 55.6 (n = 1); 1,465.7 ± 55 (n = 1); 1,343-1,322 (n = 2); 1,278.8-1,202 (n = 5); 1,167-1,153 (n = 5); 1,087-1,004 (n = 7); 993-906 (n = 19); 882.8-852 (n = 4); 269-252 (n = 4)	Present study
GR-6854	1116457	1652853	Trachyandesite	—		1,615 ± 40 (n = 1); 1,578-1,537 (n = 3); 1,487.8 ± 45 (n = 1); 1,559-1,487 (n = 3); 1,359-1,295 (n = 3); 1,266-1,199 (n = 5); 1,072-1,013 (n = 6)	Present study
U-Pb ages in previous studies							
DQB-0058r	1100929	1590508	Tuff	181 ± 1.1	1.2		González et al., 2015a
DQB-0060r	1101194	1589892	Rhyolite	180 ± 1	3.1		González et al., 2015a
DQB-0061r	1100 988	1589202	Rhyolite	177 ± 1	1.7		González et al., 2015a
ABE-oo75ra	1100882	1585343	Dacite	181 ± 4	4.5		González et al., 2015a

* Petrographic classification.

The sample GOE-1045A corresponds to a dacite according to the petrographic classification and to a trachydacite according to the chemical classification. There are two populations of zircons in this rock: one of colorless, flattened and elongated prismatic zircons (stems), with sizes ranging from 80 to 110 microns in length, and a second population of oval zircons, with sizes ranging from 20 to 100 microns. In cathodoluminescence (CL) images, the prismatic crystals show the typical oscillatory zonation of igneous zircons (Figure 8E and F), and the oval zircons correspond to inherited zircons (cathodoluminescence supplementary files). A total of 52 ablations were performed in 54 zircons (supplementary table), disregarding discordances greater than 10% in the data interpretation. The age of the entire set of zircons is calculated as 188.3 ± 2.2, with a mean square weighted deviation

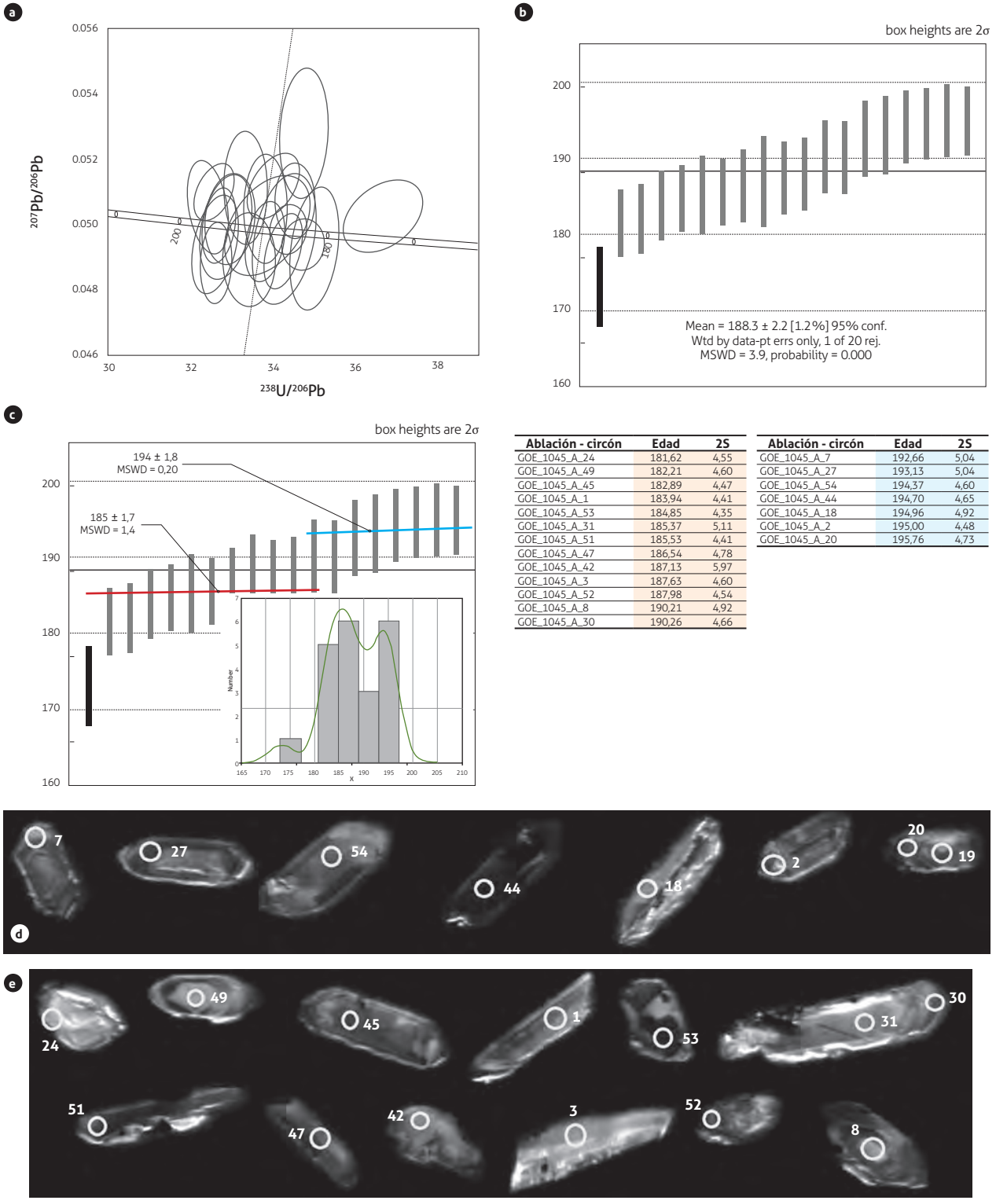

Ablación - circón	Edad	2S
GOE_1045_A_24	181,62	4,55
GOE_1045_A_49	182,21	4,60
GOE_1045_A_45	182,89	4,47
GOE_1045_A_1	183,94	4,41
GOE_1045_A_53	184,85	4,35
GOE_1045_A_31	185,37	5,11
GOE_1045_A_51	185,53	4,41
GOE_1045_A_47	186,54	4,78
GOE_1045_A_42	187,13	5,97
GOE_1045_A_3	187,63	4,60
GOE_1045_A_52	187,98	4,54
GOE_1045_A_8	190,21	4,92
GOE_1045_A_30	190,26	4,66

Ablación - circón	Edad	2S
GOE_1045_A_7	192,66	5,04
GOE_1045_A_27	193,13	5,04
GOE_1045_A_54	194,37	4,60
GOE_1045_A_44	194,70	4,65
GOE_1045_A_18	194,96	4,92
GOE_1045_A_2	195,00	4,48
GOE_1045_A_20	195,76	4,73

Figure 8. Results of U-Pb zircon dating of the sample GOE-1045A
A) Tera-Wasserburg Concordia diagram. B) Mean age. C) Mean ages of the "populations" and tables of the ages of each zircon. Black vertical bars correspond to values rejected by the Isoplot software in the mean age calculations. The age of the likely antecrystals is indicated in blue, and the crystallization age of the younger rock zircons is indicated in red. D) Cathodoluminescence image of older zircons in the population, indicating crystallization. E) Cathodoluminescence image of younger zircons

(MSWD) = 3.9 from twenty data points (Figure 8A and B), which is interpreted as the likely rock crystallization age. The probability density diagram presents two likely populations with two different ages: the population of previous zircons of the igneous system (or antecrystals) present a mean age of 194.4 ± 1.8 with MSWD = 0.20 (n=8), and the population of younger zircons present an mean age of 185.7 ± 1.7 with MSWD = 1.4 (n = 13), corresponding to the Pliensbachian (Figure 8C). A comparison of the cathodoluminescence images of the oldest and the youngest zircons yields no differences, which prevented us from identifying antecrystals (Figure 8D and E). Most of the ablations in the young and old zircons are applied to the crystal cores. The Th/U ratio ranges from 0.6 and 1.7. These values are in line with the typical ratios of igneous zircons (Rubatto, 2002), finding inherited zircons from the Triassic (n = 3), Neoproterozoic (n = 9), Mesoproterozoic (n = 9) and Paleoproterozoic (n = 1).

The sample GR-6851 corresponds to an andesite according to the petrographic classification and to a trachyandesite according to the chemical classification. The zircons of this rock are short, flattened, prismatic and euhedral, showing few stems and needles, with round and slightly oval ends and with sizes smaller than 100 microns, and some are fractured. In the cathodoluminescence (CL) images, the flattened crystals have oscillatory zonation, and the stems show a parallel pattern typical of igneous zircons (Figure 9D and E; supplementary file). A total of 48 ablations were performed in 55 zircons (supplementary table) disregarding discordances greater than 10% in the data interpretation. The age of the entire set of zircons is 188.3±2.5, with MSWD = 6.6 from twenty-two data points (Figure 9A and B), which is interpreted as a likely rock crystallization age. The probability density diagram presents two probable populations with two different ages: the population of the previous zircons of the igneous or anticrystal system present a mean age of 191.6 ± 1.7 with MSWD = 2 (n=16), and the population of younger zircons present an average age of 181.2 ± 1.7 with MSWD = 1.4 (n = 6), which corresponds to the Pliensbachian (Figure 9C). A comparison of the cathodoluminescence images of the oldest and youngest zircons yields no differences, which prevented us from identifying any antecrystals (Figure 9D and E). Most of the ablations in the young and old zircons are applied to the crystal cores, and the crystals subjected to multiple ablations yield very similar ages for the rims and cores. The Th/U ratio ranges from 0.58 to 1.6, which is in line with the typical ratios of igneous zircons (Rubatto, 2002), demonstrating inherited zircons from the Triassic (n = 4), Neoproterozoic (n = 4), Mesoproterozoic (n = 2) and Paleoproterozoic (n = 1).

The sample GR-6849 corresponds to a tuff according to the petrographic classification and to a rhyolite according to the chemical classification. The zircons of this rock correspond to two populations: one of short and stem-like, inequigranular, prismatic and euhedral crystals and another of sparse subrounded zircons of oval shapes. In the cathodoluminescence (CL) images, the prismatic crystals show oscillatory zonation, and some have inherited cores; the stem-like crystals show the typical parallel arrangement of igneous zircons. A total of 61 ablations were performed on 51 zircons (supplementary table), and discordances greater than 10% were disregarded in the data interpretation. A single weighted average age of 179.5 ± 2.1 with MSWD = 4.3 is assessed from 28 data points. This age is interpreted as the rock crystallization age and corresponds to the Toarcian (Figure 10A and B). The Th/U ratio ranges from 0.6 to 1.7, which is in line with the typical ratios of igneous zircons (Rubatto, 2002), demonstrating inherited zircons from the Permian (n = 1), Neoproterozoic (n = 11), Mesoproterozoic (n = 7) and Paleoproterozoic (n = 2).

Sample GZ-6903 corresponds to a dacite according to the petrographic classification. The zircons of this rock are part of at least two populations: one of short prismatic euhedral crystals with a few stem-like equigranular crystals and the other of oval zircons. In the cathodoluminescence (CL) images, the prismatic crystals demonstrate the oscillatory zonation typical of igneous zircons, and the oval crystals seem to have metamorphic overgrowths. A total of 69 ablations were performed in 50 zircons (supplementary Table), and discordances greater than 10% were disregarded in the data interpretation. A single weighted average age of 175.2 ± 2.3 with MSWD = 1.02 is calculated from nine data points, which is interpreted as the rock crystallization age and corresponds to the Aalenian (Figure 10C and D). The Th/U ratio ranges from 0.57 and 1.5, which is in line with the typical ratios of igneous zircons (Rubatto, 2002), demonstrating inherited zircons from the Triassic (n = 2), Permian (n = 2), Neoproterozoic (n = 24) and Mesoproterozoic (n = 25).

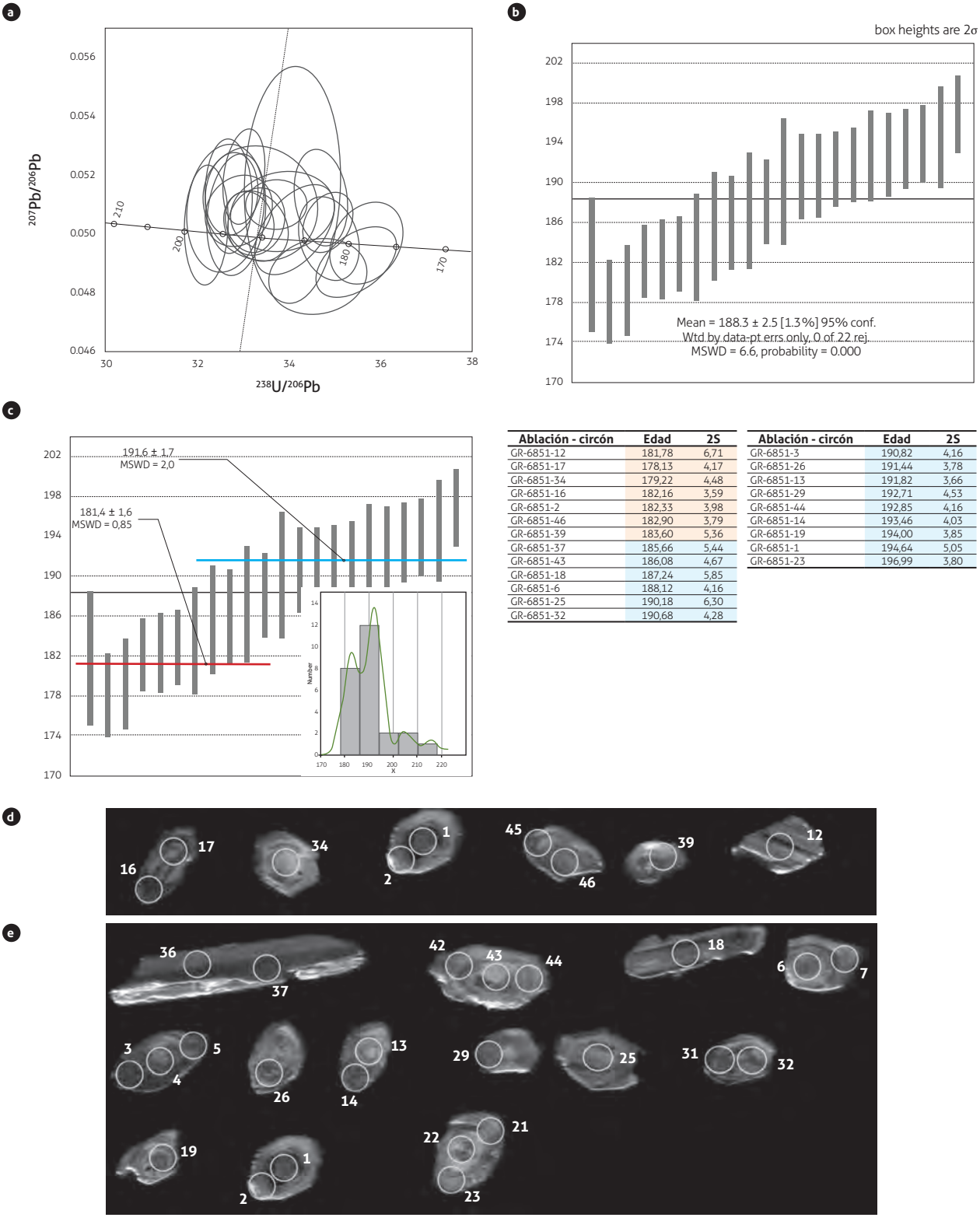

Ablación - circón	Edad	2S
GR-6851-12	181,78	6,71
GR-6851-17	178,13	4,17
GR-6851-34	179,22	4,48
GR-6851-16	182,16	3,59
GR-6851-2	182,33	3,98
GR-6851-46	182,90	3,79
GR-6851-39	183,60	5,36
GR-6851-37	185,66	5,44
GR-6851-43	186,08	4,67
GR-6851-18	187,24	5,85
GR-6851-6	188,12	4,16
GR-6851-25	190,18	6,30
GR-6851-32	190,68	4,28

Ablación - circón	Edad	2S
GR-6851-3	190,82	4,16
GR-6851-26	191,44	3,78
GR-6851-13	191,82	3,66
GR-6851-29	192,71	4,53
GR-6851-44	192,85	4,16
GR-6851-14	193,46	4,03
GR-6851-19	194,00	3,85
GR-6851-1	194,64	5,05
GR-6851-23	196,99	3,80

Figure 9. Results for U-Pb zircon dating of sample GR-6851
A) Tera-Wasserburg Concordia diagram. B) Mean age. C) Mean ages of the "populations" and tables of ages of each zircon. The ages of the likely antecrystals are shown in blue, and the crystallization ages of the younger zircons are shown in red. D) Cathodoluminescence images of the younger zircons. E) Cathodoluminescence images of the older zircons of the population, indicating crystallization

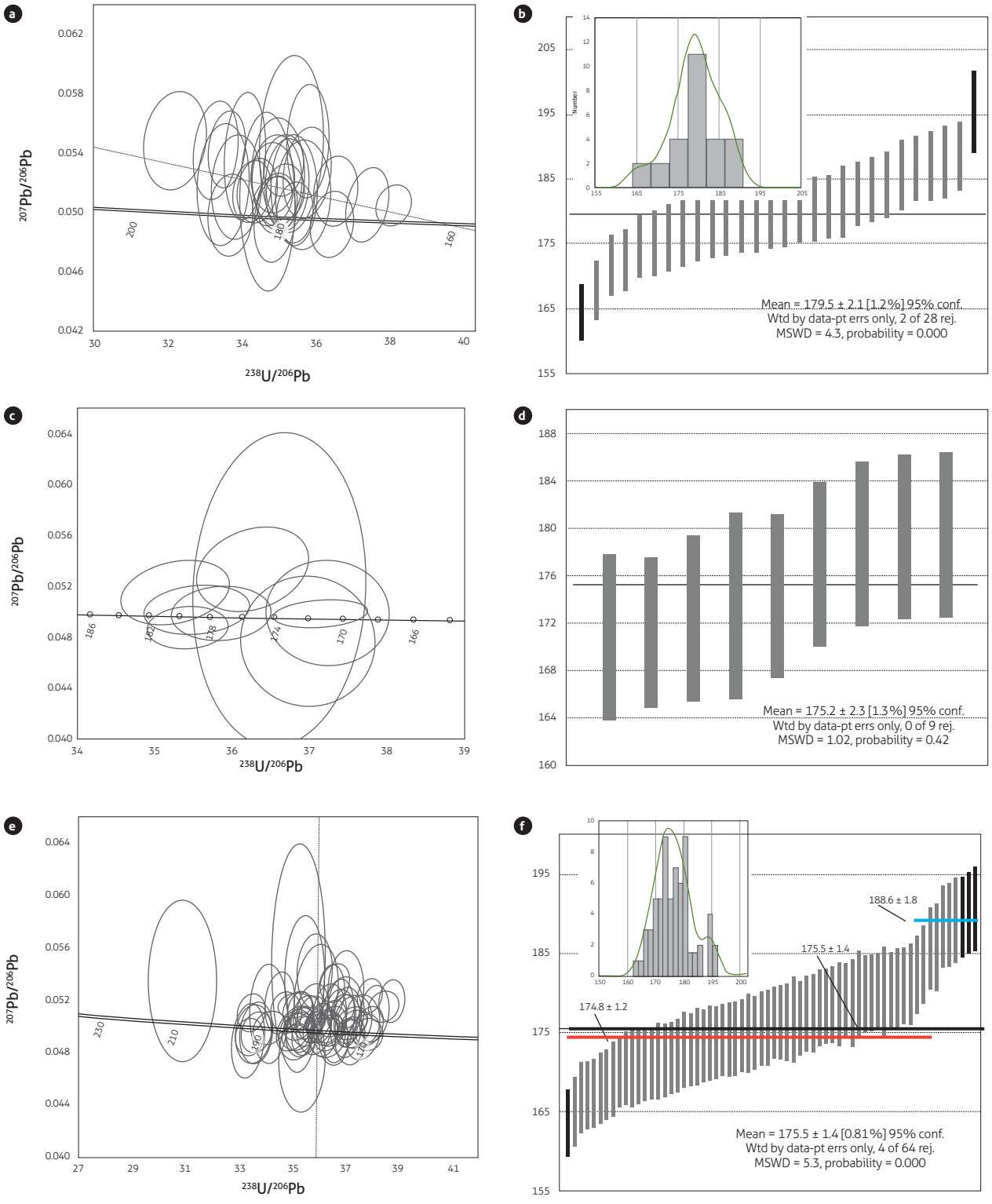

Figure 10. Results for U-Pb zircon dating
A) Tera-Wasserburg Concordia diagram of sample GR-6849. B) Mean age and probability density diagram of the zircons that define the age of sample GR-6849. C) Wetherill Concordia diagram of sample GZ-6903. D) Mean age of sample GZ-6903. E) Tera-Wasserburg Concordia diagram of sample GOE-1057. F) Mean age and probability density diagram of the zircons that define the age of sample GOE-1057 (the ages of all the zircons are shown in black; the ages of the possible antecrystals are shown in blue, and the crystallization ages of the younger zircons are shown in red). The black vertical bars in B and F correspond to values rejected by the Isoplot software in the calculation of the mean age

Sample GOE-1057 corresponds to a tuff according to the petrographic classification. The zircons of this rock are prismatic, short and equigranular, with sizes ranging from 50 to 100 microns. In the cathodoluminescence (CL) images, the zircons that define the age show oscillatory zonation, and some have complex zonation (cathodoluminescence supplementary file). A total of 94 ablations were performed in 60 zircons (supplementary table), disregarding discordances greater than 10% in the data interpretation. The age of the entire set of zircons is 175.5 ± 1.4 with MSWD = 5.3, as assessed from 64 data points (Figure 10E and F), which is interpreted as the likely rock crystallization age. The probability density diagram shows two likely populations with two different ages (Figure 10E): the population of previous zircons of the igneous system or antecrystals yields a mean age of 188.6 ± 1.8 with MSWD = 0.51 (n=8), and the population of younger zircons yields a mean age of 174.8 ± 1.2 with MSWD = 3.4 (n = 56), corresponding to the Aalenian (Figure 10F). A comparison of the cathodoluminescence images of the young and old zircons shows that the oldest ages are found for crystal rims or in fractured crystals, and some crystals have younger cores (cathodoluminescence supplementary file, supplementary table). The Th/U ratio ranges from 0.51 to 2.26, which is in line with the ratios typical of igneous zircons (Rubatto, 2002), demonstrating inheritances from the Triassic (n = 1), Neoproterozoic (n = 2) and Mesoproterozoic (n = 1).

6.1 Inheritances

To determine the populations of inherited zircons in the volcanic rocks of the La Quinta Formation, the inheritance results of six samples dated using the U-Pb zircon method are considered (GOE-1045a, GR-6851, GR-6849, GZ-6903, GOE-1057 and GR-6854); the ages of each sample are integrated and grouped. Data with discordances > 10% up to 800 Ma and discordances > 5% in ages older than 800 Ma are disregarded, leaving 112 data points that meet the condition for analysis.

The inheritances of each sample are shown in the Concordia diagrams of Figure 11, which includes the samples that do not meet the concordance criteria. The populations of inherited zircons in the volcanic rocks of the La Quinta Formation are shown in Figure 12, and some zircons characteristic of these populations are shown in Figure 13. The oldest population dates back to ~1.911 Ma (n = 3), with one concordant data point and two discordant data points, and two important populations date back to the Mesoproterozoic, at ~1.549 Ma and ~1.354, with three younger populations of ~1.247 Ma, ~1.153 and ~1.068 Ma. The most representative populations of the Neoproterozoic are dated between ~983 Ma and ~871 Ma, with two younger populations between ~618 and ~553 Ma. Four concordant data points, 287.6 ± 8.2, 269.9 ± 10, 258.8 ± 10 and 251.9 ± 9.4 Ma, are identified in the Permian. The eight Triassic zircons have a mean age of 210.3 ± 5.8. The Mesoproterozoic populations have Th/U ratios below and above 0.3, which suggests that the zircons have an igneous and metamorphic basement. The Neoproterozoic populations have Th/U ratios > 0.3, which suggests that they are mostly igneous zircons (Rubatto, 2002). The Permian and Triassic zircons generally have Th/U ratio > 1 and are thus igneous zircons (Figure 12Q and R and Figure 13A and B).

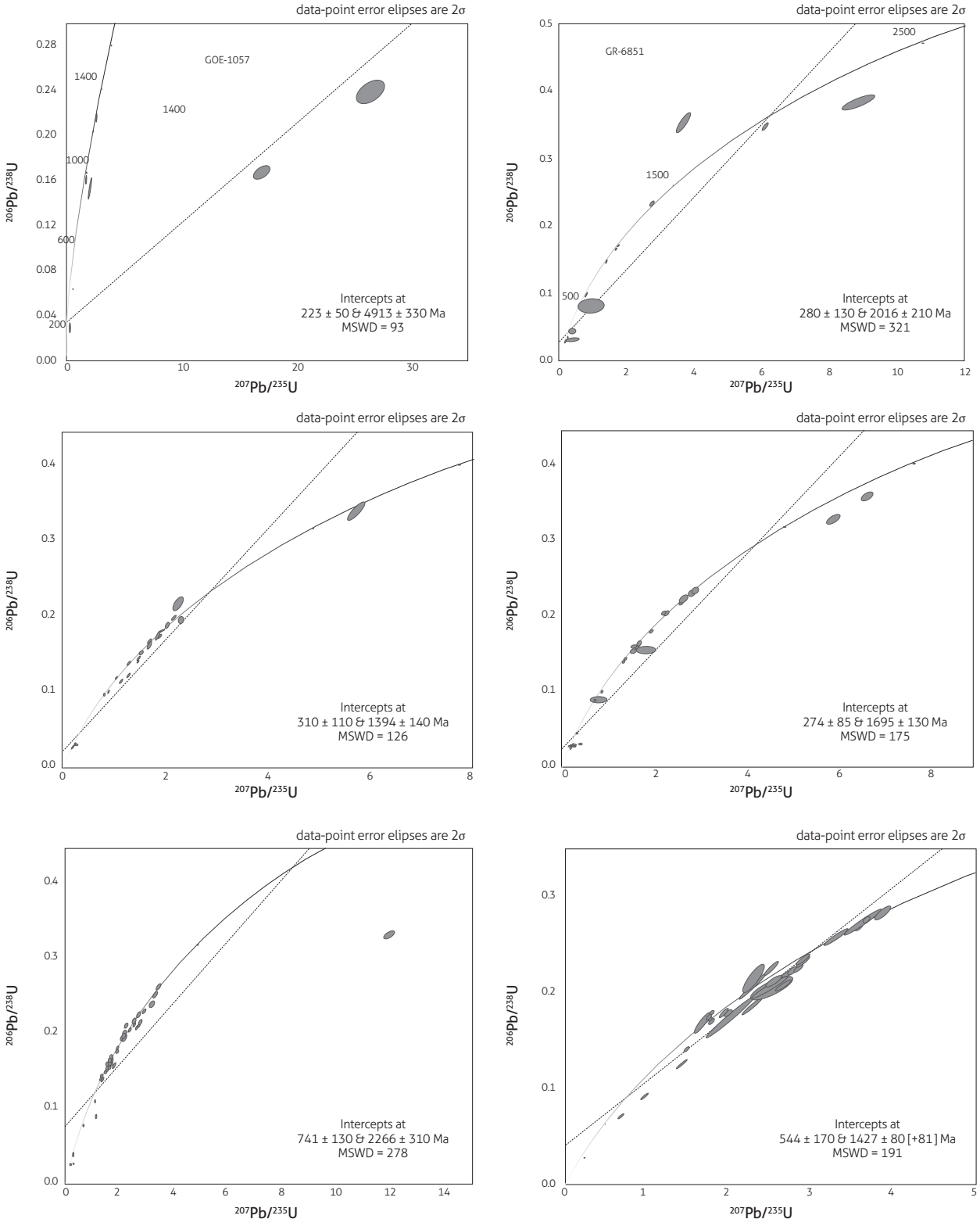

Figure 11. Concordia diagrams with all inherited age data per sample

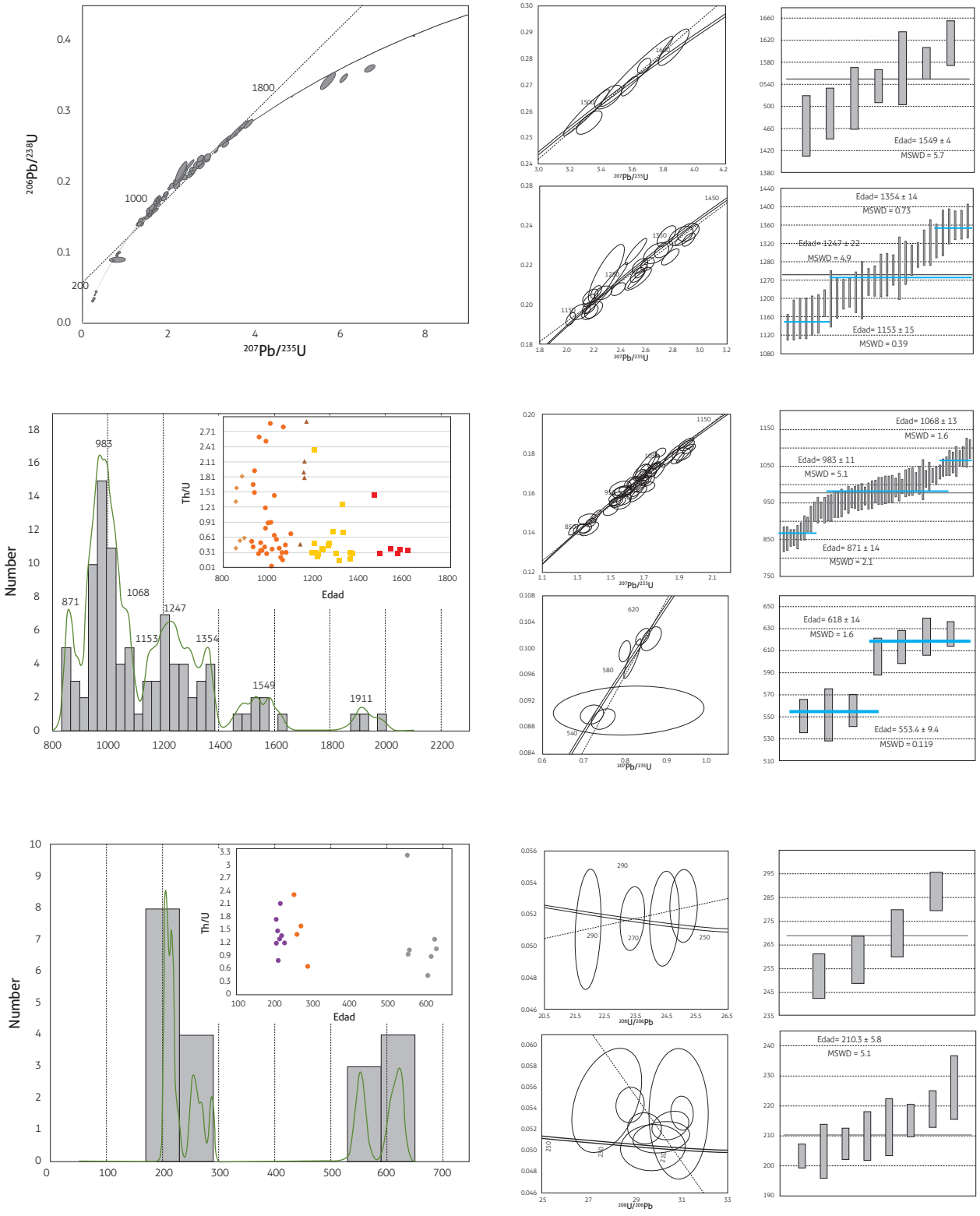

Figure 12. U/Pb geochronology of inherited zircons of the La Quinta Formation. Concordia, probability density, weighted average age and Th/U vs. age diagrams

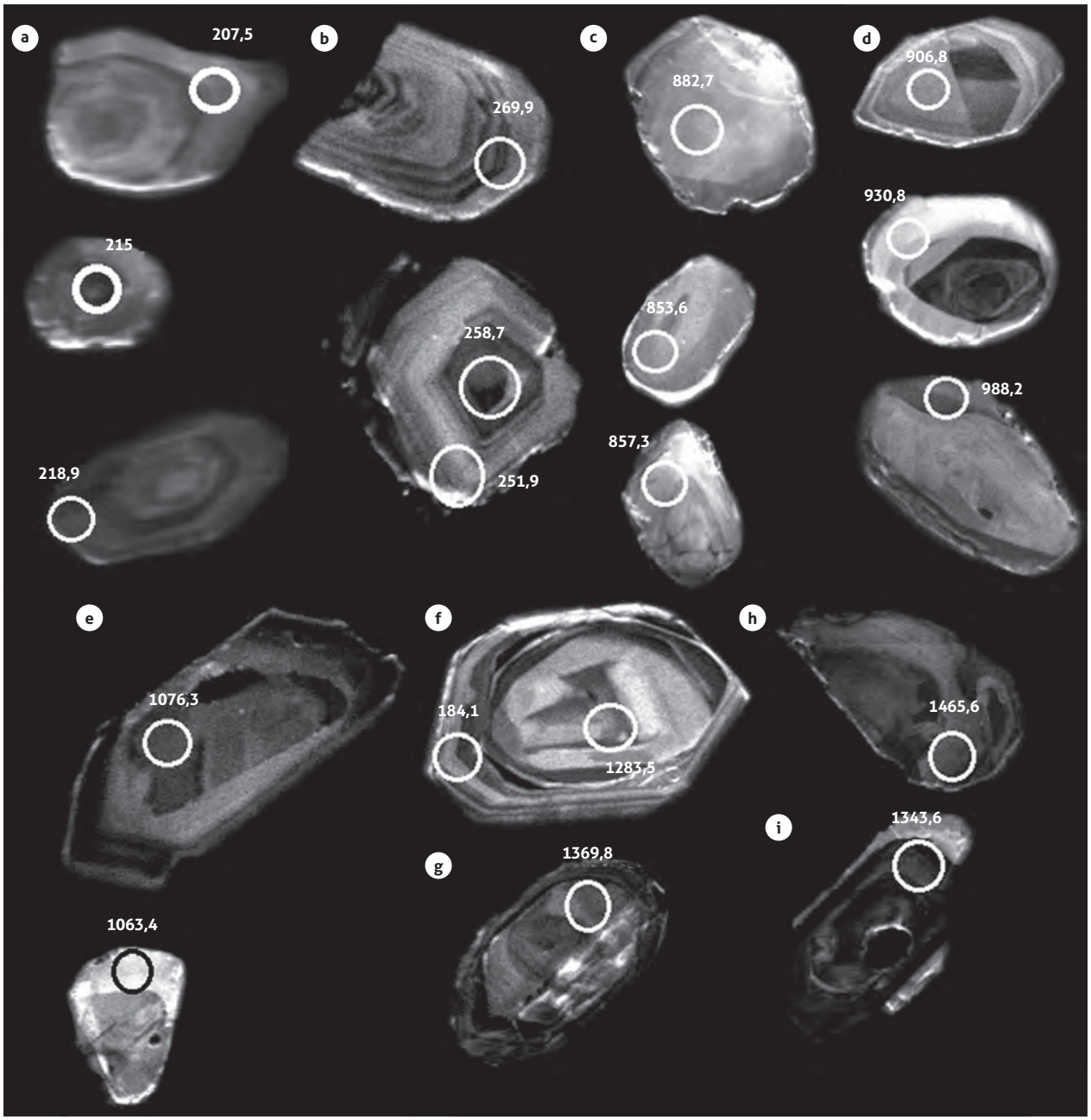

Figure 13. Cathodoluminescence images of representative xenocrystals from different populations
A and B) Triassic and Permian igneous xenocrystals with concentric texture. C) Homogeneous luminescent xenocrystals with weak internal structure. D) Crystals with metamorphic overgrowth rims around inherited cores. E) Inherited cores truncated by concentric and clear growth rims. F, G, H, I) Mesoproterozoic inherited nuclei, in some cases, with Jurassic igneous rims

7. Discussion

7.1 Ages and correlations

The crystallization ages assessed in some samples show high dispersion in the data, which suggests the presence of older zircons (antecrystals) or Pb loss. The zircon structure, shape and texture, which determine the crystallization age, show no differences according to the cathodoluminescence images for their differentiation.

The Pb^{206}/U^{238} ages that determine the crystallization of samples GOE-1045A and GR-6851 range from ~15 Ma to ~18 Ma. Most of these ages are assessed in zircon cores, with similar ages for the rims and cores when tested, suggesting that the differences in age do not result from Pb loss. Thus, these two samples likely contain a population of antecrystals, and the crystallization age is represented in the younger population; however, the information is considered insufficient, and therefore, the crystallization age of these two rocks is that of the entire population that meets the selection criteria described above. Sample GOE-1057 has a population of older ages (nine data points), which are located on the rims of zircon crystals and on zircons with internal fracturing, with younger ages in the cores of some zircons than on the rims, suggesting Pb loss and the absence of antecrystals at these more remote ages. For this reason, we consider the crystallization age of this sample to be 174.8 ± 1.2 Ma with MSWD = 3.4 and hence slightly younger than the weighted average age of the entire population, removing these eight ages from the calculation.

The data from this study indicate that the volcanism of the La Quinta Formation, in the Perijá mountain range, was active from the Lower to the Middle Jurassic. The ages suggest that the volcanism began in ~191 Ma (samples GOE-1045A and GR-6851) and continued until at least ~163 Ma (according to the U-Pb age reported by Barret et al., 2008 in Venezuela), with at least three likely periods of volcanic activity: ~188 Ma, ~179-181 Ma and ~173-175 Ma, which correspond to the crystallization ages of the rocks of the La Quinta Formation (Table 4). A comparison of the duration and episodes of crystallization of the volcanic rocks in units correlated with the La Quinta Formation, and which are part of this arc, such as the Jurassic vulcanites of the Sierra Nevada de Santa Marta (Quandt et al., 2018; Rodríguez et al., 2019b), Noreán Formation (Correa et al., 2019) and Saldaña Formation (Rodríguez et al., 2016), shows that the period of volcanic activity is virtually the same in the different volcanic units that make up the arc or fall within the crystallization period of the arc (Table 5). Furthermore, this period matches the duration of plutonism described by Rodríguez et al. (2018) and Rodríguez et al. (2020) in VSM and in SNSM. Although the geochronological data collected in the La Quinta Formation are not abundant, the petrographic and chemical composition of the rocks and the U-Pb ages suggest that the volcanism of the La Quinta Formation evolved from basic to acidic and from metaluminous to peraluminous, initially generating lava flows of basaltic trachyandesites and subsequently trachyandesites and dacites and ultimately becoming explosive and generating rhyolites and rhyolitic pyroclastic rocks in this region. This volcanism occurred in a subaerial setting, developing hematite, which stained the rocks a reddish color. The dates estimated in previous studies using the U-Pb method on volcanic rocks indicate ages ranging from 176 to 182 Ma (González et al., 2015 a, b) on the western flank of the Perijá mountain range and of 163 ± 5 Ma in Venezuela (Dasch, 1982). Barrett et al. (2008) located this unit between the Lower and Middle Jurassic, according to fossil evidence of *Ornithischian Lesothosaurus* sp. and reptile remains (in Nova et al., 2012).

The comparison of the geochronology, geochemistry and petrography results of this study with those reported for the Noreán Formation of the Santander massif in the San Lucas mountain range (Ingeominas-UIS, 2006a, 2006c, 2006d, 2006e; Leal Mejía, 2011; González et al., 2015a, 2015b and Correa Martínez et al., 2019), for the volcanic units of Sierra Nevada de Santa Marta (Guatapurí and Corual formations, Caja de Ahorros, La Paila and Los Clavos ignimbrites, Los Tábanos Triassic spilites, keratophyric porphyries and rhyodacites and Golero rhyolites) (Tschanz et al., 1969a; Maze, 1984; Quandt et al., 2018, Rodríguez et al., 2019c), for Ipapure-Cerro de La Teta rhyodacites in Upper Guajira (Radelli, 1960; Rodríguez and Londoño, 2002; Zuluaga et al., 2015) and for the Saldaña Formation and Pitalito vulcanites in the Upper Magdalena Valley (Rodríguez et al., 2016; Zapata et al., 2016) shows that all the volcanic rocks of these units are correlated with the volcanic rocks of the La Quinta Formation.

Table 5. Comparison between the crystallization period of volcanic arc units and periods of increased crystallization, based on U-Pb zircon ages

Lithological unit	Activity lapse	Crystallization episodes	Source
Saldaña Formation and Pitalito vulcanites	~190 to ~164 Ma	~190-186 Ma, ~183-178 Ma, ~173-168 Ma	Rodríguez et al. (2016)
Noreán Formation	~194 to ~175 Ma	~192 Ma, ~185 Ma, ~175 Ma	Correa et al. (2019)
Volcanic units of SNSM	~196 to ~165 Ma	~195 Ma, ~186 Ma, ~178-175 y ~168 Ma	Rodríguez et al. (2019b)
La Quinta Formation	~196 to ~164 Ma	~188 Ma, ~179-181 Ma, ~173-175 Ma	Present study
Cerro de La Teta and Ipapure rhyodacites	~ 184 to ~181		Zuluaga et al. (2015)

The U-Pb zircon geochronology results of the volcanic units show similar crystallization periods and geochemical behavior of major and trace elements suggesting that they were formed from the same continental volcanic arc (Rodríguez et al., 2016; 2018, 2019b, Correa et al, 2019, Quandt et al., 2018), which was subsequently dispersed along the paleomargin of northern South America (Bayona et al., 2010; Villagómez et al., 2015; Zapata et al., 2016; Zuluaga et al., 2015, Rodríguez et al., 2019a).

7.2 Inheritance and basement

The presence of xenocrystals and inherited zircon cores in the rocks of the La Quinta Formation is most likely related to the melting of older wall rocks. This process commonly occurs in magmatic systems. The formation of antecrystals, which is more debatable and difficult to determine, was found in some of the rocks analyzed in this study, which is in line with the crystallization episodes of the arc (Table 5).

The ages of the inherited zircons in the volcanic rocks of the La Quinta Formation match the ages and inheritances described by Ibáñez Mejía et al. (2015) for the Putumayo orogen. These authors suggest that the inherited zircons with ages older than 0.9 Ga possibly derived from metasedimentary rocks of the Mesoproterozoic basement and were contributed to by an older Cratonic domain. In our case, the inherited zircons were incorporated into Jurassic magmas, which produced the La Quinta Formation, among others, through melting of the Putumayo orogen crust. Ages between 1.15 and 1.10 Ga, according to Ibáñez Mejía et al. (2015), are associated with accretion of arc edges against the continental margin, triggering an early metamorphic event, and ages of approximately 0.99 Ga have been interpreted as the Amazonia incorporation into the core of Rodinia during the collision with the Baltic (Ibáñez Mejía et al., 2015). This would largely explain the oldest inheritances of the volcanic arc of 0.9 Ga, which would be contributed to the arc by the basement of the Putumayo orogen that belongs to the Chibcha Terrane (Restrepo et al., 2009). This terrane currently spans across part of the Cordillera Oriental [Eastern Ranges] and the easternmost section of the Cordillera Central [Central Andes] and consists of a Neoproterozoic crystalline basement (Putumayo orogen), Paleozoic marine sedimentary sequences and intrusions and volcanic rocks of arcs formed during the Carboniferous-Permian and the Lower-to-Middle Jurassic. After the formation of the arcs, the Chibcha Terrane was divided into blocks scattered along the paleomargin of northern South America, as we currently know it (Rodríguez et al., 2019a).

The ages of 618 and 553 Ma are similar to the inheritances described by Rodríguez et al. (2019a) in the plutons of the Permian arc, which, according to Nova et al. (2018), possibly correspond to the zircons of units included in the Mixteco and Maya blocks of Mexico. The source of the Triassic igneous xenocrystals is unknown; most likely, they are related to minor igneous bodies still unidentified in the Chibcha Terrane and in general older than plutonic rocks of intrusions dated between the Triassic and the Lower Jurassic of the Santander massif.

A comparison of the ages of the xenocrystals and inherited zircon cores of the La Quinta Formation with other correlated volcanic units suggests that all these volcanic units have similar zircon inheritance, which would indicate that they shared the same preexisting basement, on which all the arc units were emplaced: the Noreán Formation has zircon inheritances from the Mesoproterozoic (~1400 Ma, n = 1) and from the period between the Mesoproterozoic and Neoproterozoic (~1.050 and 950 Ma, n = 3) (Correa Martínez et al., 2019); the Saldaña Formation has inheritances from the Mesoproterozoic (~1.460, ~1.570 and ~1.630 Ma), Neoproterozoic

(~906 to ~1.060 Ma and ~510 Ma), Permian (~270 Ma) and Triassic (~223 Ma) (Rodríguez et al., 2016; Zapata et al., 2016); the Jurassic volcanic rocks of the Sierra Nevada de Santa Marta have Mesoproterozoic, Neoproterozoic, Paleozoic, Permian and Triassic xenocrystals, as well as ages contemporary with Pan-African orogeny events during the Devonian (400-650 Ma) (Rodríguez et al., 2019c).

7.3 Tectonic model

Different arc models have been proposed for Jurassic magmatism: Bayona et al. (2010), based on paleomagnetic data, consider that blocks moved northward relative to a point on the craton and formed an oblique-subduction margin along the South American paleomargin. Villagómez et al. (2015), similar to Bayona et al. (2010), conclude that the Jurassic blocks of the Upper Magdalena, Cordillera Central [Central Andes], San Lucas mountain range and Sierra Nevada de Santa Marta are allochthons formed in an arc and in a back-arc and the Jurassic rocks of the Santander massif are autochthonous and related to a rift; Spikings et al. (2015) postulate that the westward shift in Jurassic magmatism over time is due to slab rollback and/or trench retreat; Bustamante et al. (2016) and Quandt et al. (2018) embrace the idea of highly oblique subduction; the former explain the compositional changes by reduced sediment melting and long-term source evolution (proposed by Leal Mejía, 2011); Zapata et al. (2016) consider the volcanic and plutonic rocks to share the same arc history and to be related to a fragmented Jurassic magmatic belt; Zuluaga et al. (2015) discuss the relationship between the plutons and Jurassic volcanic rocks of La Guajira and conclude that they were formed in the same axis, which would imply that there was no back-arc and that they formed within the arc; Rodríguez et al. (2018) consider the arc to be represented by volcanic and plutonic rocks that were formed in the Upper Magdalena Valley during three high-activity magmatic pulses (from 188 to 186 Ma, from 183 to 178 Ma and from 173 to 168 Ma), that the plutons tended to rejuvenate from west to east, that the north of the Ibagué Batholith is not part of this arc and that this batholith was emplaced in an Upper Jurassic orogen (Blanco Quintero et al., 2014, Rodríguez et al., 2020). These authors attribute the compositional changes and the migration of the plutons to erosion of the accretionary prism due to the increased water flow from the subduction slab, consequently decreasing the *solidus* temperatures; Rodríguez et al. (2020) propose three magmatic arcs for the Jurassic magmatism of the northern Andes, each one formed at different periods, with their own chemical and petrographic composition and emplaced in different orogens.

The geochemistry and geochronology data presented here show the correlation between the volcanic units that make up the different blocks of the northern Andes (Saldaña Formation, Pitalito vulcanites, Noreán Formation, SNSM Jurassic volcanic units, La Quinta Formation and Cerro de La Teta and Ipapure rhyodacites), which suggests that from Ecuador through the Upper Magdalena Valley to La Guajira, volcanism was generated in a similar time span of ~30 Ma, from 195 Ma to 164 Ma, and that the pulses or episodes of peak magmatic activity were virtually identical in these units and in their plutonic equivalents, in contrast to an oblique subduction model, considering multiple arcs.

According to some authors, the Jurassic units correspond to a single arc that evolved from east to the west over an extended period of time. Based on the above, oblique subduction is postulated considering the Jurassic plutonism and volcanism data of the Upper Magdalena Valley (Rodríguez et al., 2016, Zapata et al, 2016; Bustamante et al., 2016; Rodríguez et al., 2018), San Lucas mountain range (Leal Mejía, 2011; Correa et al., 2019), Sierra Nevada de Santa Marta (Tschanz et al., 1969a; Quandt et al., 2018 y Rodríguez et al., 2019b) and Upper Guajira (Zuluaga et al., 2015), which show similar composition and spatial behavior and considerably different chemical and petrographic composition from the Triassic-Jurassic units of the Santander massif (Rodríguez et al., 2017, 2020) and from the north of the Ibagué Batholith.

The analysis of the data of the Upper Magdalena Valley and Sierra Nevada de Santa Marta shows coincidences when describing the compositional variation in the plutons of these two blocks (Tschanz et al., 1969; Jaramillo and Escovar, 1980; Núñez et al., 1996), corroborating published petrographic and geochemical results (Rodríguez et al., 2018 y Rodríguez et al., 2019b). The studies by Jaramillo and Escovar (1980) and by Núñez et al. (1996) describe eastward macroscopic and compositional changes in plutons in the Upper Magdalena Valley and show

that the bodies are more acidic and granitic in the same direction. Tschanz et al. (1969) separated the plutons of Sierra Nevada de Santa Marta into two batholith belts, a central belt and southeastern belt, and they described their macroscopic differences, stating that the southeastern belt was granitic.

In this context and considering the volume of information published, the arc to which the La Quinta Formation belongs shows eastward compositional and temporal migration that was most likely caused by erosion of the trench subduction front as the Farallones plate slid under the continental paleomargin during the ~30 Ma years of the duration of the arc. This continental arc is characterized by erosion, with eastward compositional migration and rejuvenation.

The continental margin, in the northern Andes, has been an accretion margin of blocks or terranes. Much of this accretion is represented by the metamorphic sequences of the Cordillera Central [Central Andes] and by the volcanic rocks of the Cordillera Occidental [West Andes]. In some periods, the margin has behaved as an erosional margin. In this study, the margin was considered erosional between the Lower and Middle Jurassic, during the formation of this Jurassic arc.

8. Conclusions

The La Quinta Formation is a volcano-sedimentary unit composed mainly of detrital sedimentary rocks (conglomerates, sandstones and mudstones) and subordinate chemical sedimentary (limestones) and extrusive and pyroclastic volcanic rocks. The extrusive rocks have a basaltic, andesitic, dacitic and rhyolitic composition, and the pyroclastic rocks are crystal-vitreous and lithic tuffs of ash and lapilli size and agglomerates. The chemical classification of the extrusive rocks based on higher oxides matches the modal classification. The tuffs are chemically classified as dacites and rhyolites.

The chemistry results from this study and from previous studies indicate that the volcanic rocks were formed in a subduction-related setting in a volcanic-plutonic arc with compositional variations and eastward rejuvenation related to an erosional continental margin arc.

The ages suggest that the volcanism began in ~191 Ma (Sinemurian) and continued until ~164 Ma, with at least three periods of increased volcanic activity: 186 Ma (Pliensbachian), 179-181 Ma (Toarcian) Ma and 173-175 (Toarcian), and continued until the Middle Jurassic (Callovian).

The periods of peak volcanic activity are correlated with similar periods in volcanic units during the Lower and Middle Jurassic in the Upper Magdalena Valley (Saldaña Formation and Pitalito Vulcanites), the San Lucas mountain range (Noreán Formation), Sierra Nevada de Santa Marta (Guatapurí and Corual formations, Caja de Ahorros, La Paila and Los Clavos ignimbrites, Triassic spilites, keratophyric porphyries, Los Tábanos Rhyodacite and Golero Rhyolite), and the Cocinas mountain range (Ipapure-Cerro La Teta Rhyodacite). All these units, including the La Quinta Formation, have similar chemical and petrographic compositions; in these units, the inherited zircons mark similar populations and were formed from the same Plutonic volcanic arc along the South American paleomargin on a crystalline basement consisting of Neoproterozoic rocks, Paleozoic sedimentary units and Permian arc plutons, which appear in tectonic blocks as we know them today.

The lack of xenocrystals with Ordovician ages in all the correlated volcanic units of the Lower and Middle Jurassic indicates that the La Quinta Formation did not develop in the basement of the Famatinian orogen of the Santander massif but was instead established in rocks of the Neoproterozoic basement of the Putumayo orogen and in intrusions of the Permian arc predating the Lower and Middle Jurassic arc.

Acknowledgments

We would like to thank the Servicio Geológico Colombiano for funding the project, the SGC Petrography and Chemistry laboratories for preparing the thin sections and for the chemical analyses of the samples, respectively, the SGC Geochronology Laboratory for the U-Pb zircon dating of six samples, the geologist Gilberto Zapata for his help with field sampling, Tomás Correa for translating the abstract of the article, Juan Pablo Zapata for making the figure of the general geological map, and the reviewers for their comments, which allowed us to improve the manuscript.

References

Arias, A., & Morales, C. (1999). *Geología del departamento de Cesar*. Bogota: Ingeominas.

Barrett, M., Butler, R., Moore-Fay, S., Novas, F., Moody, J., Clark, J., & Sánchez-Villagra, M. (2008). Dinosaur remains from the La Quinta Formation (Lower or Middle Jurassic) of the Venezuelan Andes. *Paläontologische Zeitschrift*, 82, 163-177. https://doi.org/10.1007/BF02988407

Bayona, G., Jiménez, G., Silva, C., Cardona, A., Montes, C., Roncancio, J., & Cordani, U. (2010). Paleomagnetic data and K–Ar ages from Mesozoic units of the Santa Marta massif: A preliminary interpretation for block rotation and translations. *Journal of South American Earth Sciences*, 29 (4), 817-831. https://doi.org/10.1016/j.jsames.2009.10.005

Blanco Quintero, I. F., García Casco, A., Toro, L. M., Moreno, M., Ruiz, E. C., Vinasco, C. J., & Morata, D. (2014). Late Jurassic terrane collision in the northwestern margin of Gondwana (Cajamarca Complex, eastern flank of the Central Cordillera, Colombia). *International Geology Review*, 56 (15), 1852-1872. https://doi.org/10.1080/00206814.2014.963710

Bustamante, C., Cardona, A., Bayona, G., Mora, A., Valencia, V., Gehrels, G., & Vervoort, J. (2010). U-Pb LA-ICP-SM Geochronology and regional correlation of middle Jurassic intrusive rocks from the Garzon massif, upper Magdalena valley and Central cordillera, southern Colombia. *Boletín de Geología*, 32 (2), 93-109.

Bustamante, C., Archanjo, C., Cardona, A., Valencia, V., & Vervoort, J. (2016). Late Jurassic to Early Cretaceous plutonism in the Colombian Andes: a record of long-term arc maturity. *GSA Bulletin*, 128 (11-12), 1762-1779 https://doi.org/10.1130/B31307.1.

Cano, N. A., Molano, J. C., Guerrero, N. M., Sepúlveda, M. J., Prieto, D., Murillo, H., & Patiño, R. (2017). Petrología de los miembros volcánicos de la Formación La Quinta. Abstracts. XVI Congreso de Geología. Santa Marta.

Cediel, F., Mojica, J., & Macía, C. (1980). Definición estratigráfica del Triásico en Colombia, Suramérica. Formaciones Luisa, Payandé y Saldaña. *Newsletters on Stratigraphy*, 9 (2), 73-104. https://doi.org/10.1127/nos/9/1980/73

Cediel, F., Mojica, J., & Macía, C. (1981). Las formaciones Luisa, Payandé y Saldaña: sus columnas estratigráficas características. *Geología Norandina*, 3, 11-19.

Condie, K. C., & Kröner, A. (2013). The building blocks of continental crust: Evidence for a major change in the tectonic setting of continental growth at the end of the Archean. *Gondwana Research*, 23 (2), 394-402. https://doi.org/10.1016/j.gr.2011.09.011

Correa Martínez, A. M., Rodríguez, G., Arango, M. I., & Zapata García, G. (2019). Petrografía, geoquímica y geocronología U-Pb de las rocas volcánicas y piroclásticas de la Formación Noreán al NW del macizo de Santander, Colombia. *Boletín de Geología*, 41 (1), 29-54. https://doi.org/10.18273/revbol.v41n1-2019002

Coyner, S. J., Kamenov, G. D., Mueller, P. A., Rao, V., & Foster, D. A. (2004). FC-1: A zircon reference standard for the determination of Hf isotopic compositions via laser ablation ICP-MS. *American Geophysical Union, Fall Meeting.* San Francisco.

Dasch, L. E. (1982). *U-Pb geochronology of the Sierra de Perijá* (Ph. D. thesis). Case Western Reserve University.

Forero, S. (1970). Estratigrafía del Precámbrico en el flanco occidental de la serranía de Perijá. *Geología Colombiana*, 7, 7-78.

Forero, A. (1972). Estratigrafía del Precretácico en el flanco occidental de la serranía de Perijá. *Geología Colombiana*, 7, 7-78.

Geoestudios. (2006). Cartografía geológica cuenca Cesar-Ranchería. Final inform.

Girardi, V. A. V., Teixeira, W., Bettencourt, J. S., Andrade, S., Navarro, M. S., & Sato, K. (2008). Trace element geochemistry and Sr-Nd characteristics of Mesoproterozoic mafic intrusive rocks from Rondônia, Brazil, SW Amazonian craton: Petrogenetic and tectonic inferences. *Episodes*, 31 (4), 392-400. https://doi.org/10.18814/epiiugs/2008/v31i4/004

González, H., Maya, M., Camacho, J., Cardona, O. D., & Vélez, W. (2015a). *Elaboración de la cartografía geológica de un conjunto de planchas a escala 1:100.000 ubicadas en cuatro bloques del territorio nacional, identificados por el Servicio Geológico Colombiano. Plancha 41: Becerril*. Bogota: Servicio Geológico Colombiano.

González, H., Maya, M., García, J. F., Gómez, J. P., Palacio, A. F., & Vélez, W. (2015b). *Elaboración de la cartografía geológica de un conjunto de planchas a escala*

1:100.000 ubicadas en cuatro bloques del territorio nacional, identificados por el Servicio Geológico Colombiano. Plancha 42: serranía de Perijá. Bogotá: Servicio Geológico Colombiano.

Hernández, M. (2003). *Memoria explicativa geología plancha 48, Jagua de Ibirico. Esc 1:100.000*. Bogotá: Ingeominas.

Hellstrom, J., Paton, C., Woodhead, J. D., & Hergt, J. M. (2008). Iolite: Software for spatially resolved LA-(quad and MC) ICP-MS analysis. In: P. Sylvester (ed.), *Laser Ablation ICP-MS in the Earth sciences: Current practices and outstanding issues* (pp. 343-348). Vancouver: Mineralogical Association of Canada.

Hughes, C. J. (1972). Spilites, keratophyres and the igneous spectrum. *Geological Magazine,* 109 (6), 513-527. https://doi.org/10.1017/S0016756800042795.

Ibáñez Mejía, M., Pullen, A., Arenstein, J., Gehrels, G., Valley, J., Ducea, M., Mora, A., Pecha, M., & Ruiz, J. (2015). Unraveling crustal growth and reworking processes in complex zircons from orogenic lower-crust: The Proterozoic Putumayo Orogen of Amazonia. *Precambrian Research*, 267, 285-310. https://doi.org/10.1016/j.precamres.2015.06.014

Ingeominas. (2002). *Atlas geológico digital de Colombia. Versión 1.1, plancha 5-06. Escala 1: 500.000.* Bogotá: Ingeominas.

Ingeominas-UIS. (2006a). *Cartografía geológica de 9.600 km² de la serranía de San Lucas: planchas 55 (El Banco), 64 (Barranco de Loba), 85 (Simití) y 96 (Bocas del Rosario). Aporte a su evolución geológica*. Memoria explicativa de la Plancha 85: Simití. Bucaramanga: Ingeominas.

Ingeominas-UIS. (2006b). *Geología de la plancha 55: El Banco. Escala 1:100.000. Mapa Geológico.* Bogotá y Bucaramanga: Ingeominas.

Ingeominas-UIS. (2006c). *Cartografía geológica de 9.600 km² de la serranía de San Lucas: planchas 55 (El Banco), 64 (Barranco de Loba), 85 (Simití) y 96 (Bocas del Rosario). Aporte a su evolución geológica.* Memoria explicativa de la plancha 55: El Banco. Bucaramanga: Ingeominas.

Ingeominas-UIS. (2006d). *Cartografía geológica de 9.600 km² de la serranía de San Lucas: planchas 55 (El Banco), 64 (Barranco de Loba), 85 (Simití) y 96 (Bocas del Rosario). Aporte a su evolución geológica.* Memoria explicativa de la plancha 64: Barranco de Loba. Bucaramanga: Ingeominas.

Ingeominas-UIS. (2006e). Cartografía geológica de 9.600 km² de la serranía de San Lucas: planchas 55 (El Banco), 64 (Barranco de Loba), 85 (Simití) y 96 (Bocas del Rosario). Aporte a su evolución geológica. Memoria explicativa de la plancha 96: Bocas del Rosario. Bucaramanga: Ingeominas.

Invemar, Ingeominas, Ecopetrol, ICP y Geosearch. (2007). *Geología de las planchas 11, 12, 13, 14, 18, 19, 20, 21, 25, 26,27, 33 y 34. Proyecto: "Evolución geohistórica de la Sierra Nevada de Santa Marta"*. Bogotá: Ingeominas.

Janoušek, V., Farrow, C. M., & Erban, V. (2006). Interpretation of whole-rock geochemical data in igneous geochemistry: Introducing Geochemical Data Toolkit (GCDkit). *Journal of Petrology*, 47 (6), 1255-1259. https://doi.org/10.1093/petrology/egl013.

Jaramillo, L., & Escovar, R. (1980). *Cinturones de pórfidos cupríferos en las cordilleras colombianas. Simposio sobre metalogénesis en Latinoamérica*. 17p, México D.F.

Kundig, E. (1938). Las rocas precretáceas de los Andes centrales de Venezuela, con algunas observaciones sobre su tectónica. *Venezuela Boletín de Geología y Mine*ría, 2 (2), 3.

Leal Mejía, H. (2011). *Phanerozoic gold metallogeny in the Colombian Andes: A tectono-magmatic approach* (Ph. D. Thesis). University of Barcelona.

Leal Mejía, H., Shaw, R. P., & Melgarejo, J. C. (2019). Spatial-temporal migration of granitoid magmatism and the Phanerozoic tectono-magmatic evolution of the Colombian Andes. In: F. Cediel y R. P. Shawn (eds.), *Geology and tectonics of Northwestern South America* (pp. 253-410). Frontiers in Earth Sciences. Springer, Cham. https://doi.org/10.1007/978-3-319-76132-9_5.

Le Bas, M., Le Maitre, R., Streckeisen, A., & Zanettin, B. (1986). A chemical classification of volcanic rocks based on the total alkali-silica diagram. *Journal of Petrology*, 27 (3), 745-750. https://doi.org/10.1093/petrology/27.3.745

Le Maitre, R. W., Streckeisen, A., Zanettin, B., Le Bas, M. J., Bonin, B., Bateman, P., & Lamere, J. (2002). Igneous rocks: A classification and glossary of terms: Recommendations of the International Union of Geological Sciences. In: *Subcommission on the Systematics of Ig-*

neous Rocks. Cambridge University Press. https://doi.org/10.1017/CBO9780511535581

Ludwig, K. R. (2012). User's manual for Isoplot 3.75- 4.15. A Geochronological Toolkit Microsoft Excel. Berkeley Geochronology Center, Special Publication, 5.

Maze, W. (1984). Jurassic La Quinta Formation in the Sierra de Perijá, Northwestern Venezuela: Geology and tectonic environment of red beds and volcanic rocks. In: W. Bonini, R. Hargraves y R. Shagam (eds.). *The Caribbean-South American Plate boundary and regional tectonics* (pp. 263-282). McLean: Geological Society of America, v. 162. https://doi.org/10.1130/MEM162-p263.

Miller, J. B. (1960). Directrices tectónicas en la sierra de Perijá. *Boletín Geológico de Venezuela*, publicación especial, n.º 3, t. II.

Mojica, J., & Kammer, A. (1995). Eventos jurásicos en Colombia. *Geología Colombiana*, 19, 165-172.

Mojica, J., Kammer, A., & Ujueta, G. (1996). El Jurásico del sector noroccidental de Suramérica y guía de la excursión al valle superior del Magdalena (nov. 1-4/95), regiones de Payandé y Prado, departamento del Tolima, Colombia. *Geología Colombiana*, 21, 3-41.

Mojica, J., & Dorado, J. (1987). El Jurásico anterior a los movimientos intermálmicos en los Andes colombianos. Parte A: Estratigrafía. In: W. Volkheimer (ed.), *Bioestratigrafia de los sistemas regionales del Jurásico y Cretácico de América del Sur* (pp. 49-110). Mendoza: Comité Sudamericano del Jurásico y Cretácico, v. 1.

Nakamura, N. (1974). Determination of REE, Ba, Fe, Mg, Na and K in carbonaceous and ordinary chondrites. *Geochimica et Cosmochimica Acta*, 38 (5), 757-775. https://doi.org/10.1016/0016-7037(74)90149-5.

Nova, G., Montaño, P., Bayona, G., Rapalini, A., & Montes, C. (2012). Paleomagnetismo en rocas del Jurásico y Cretácico Inferior en el flanco occidental de la serranía del Perijá: contribuciones a la evolución tectónica del NW de Suramérica. *Boletín de Geología*, 34 (2), 117-138.

Nova, G., Bayona, G., Silva, J., Cardona, A., Rapalini, A., Montaño, P., Eisenhauer, A., Dussan, K., Valencia, V., Ramírez, V., & Montes, C. (2018). Jurassic break-up of the Peri-Gondwanan margin in Northern Colombia: Basin formation and implications for terrane transfer. *Journal of South American Earth Sciences*, 89, 92-117. https://doi.org/10.1016/j.jsames.2018.11.014

Núñez A., Bocanegra, A., & Gómez, J. (1996). Los plutones jurásicos del valle superior del Magdalena. *VII Congreso Colombiano de Geología*. Bogotá, Colombia.

Paton, C., Woodhead, J. D., Hellstrom, J. C., Hergt, J. M., Greig, A., & Maas, R. (2010). Improved laser ablation U-Pb zircon geochronology through robust downhole fractionation correction. *Geochemistry, Geophysics, Geosystems*, 11 (3), 1-36. https://doi.org/10.1029/2009GC002618.

Pastor Chacón, A., Reyes Abril, J., Cáceres Guevara, C., Sarmiento, G., Cramer, T. (2013). Análisis estratigráfico de la sucesión del Devónico-Pérmico al oriente de Manaure y San José de Oriente (serranía del Perijá, Colombia). *Geología Colombiana*, 38, 5-24.

Pearce, J. A., Harris, N. B., & Tindle, A. G. (1984). Trace Element Discrimination Diagrams for the Tectonic Interpretation of Granitic Rocks. *Journal of Petrology*, 25 (4), 956-983. https://doi.org/10.1093/petrology/25.4.956

Pearce, J. A. (1996). A user's guide to basalt discrimination diagrams. In D. A. Wyman (ed.), *Trace element geochemistry of volcanic rocks: Applications for massive sulphide exploration* (pp. 79-113). Winnipeg: Geological Association of Canada. Short Course Notes v. 12.

Pearce, J. A. (2008). Geochemical fingerprinting of oceanic basalts with applications to ophiolite classification and the search for Archean oceanic crust. *Lithos*, 100 (1-4), 14-48. https://doi.org/10.1016/j.lithos.2007.06.016.

Peña Urueña, M. L., Muñoz Rocha, J. A., & Urueña, C. L. (2018). Laboratorio de Geocronología en el Servicio Geológico Colombiano: avances sobre datación U-Pb en circones mediante la técnica LA-ICP-MS. *Boletín Geológico*, 44, 39-56. https://doi.org/10.32685/0120-1425/boletingeo.44.2018.7

Petrus, J. A., & Kamber, B. S. (2012). Vizual age: A novel approach to laser ablation ICP-MS U-Pb geochronology data reduction. *Geostandards and Geoanalytical Research*, 36 (3), 247-270. https://doi.org/10.1111/j.1751-908X.2012.00158.x.

Peccerillo A., & Taylor, T. S. (1976). Geochemistry of Eocene calc-alkaline volcanic rocks from Kastamonu area, Northern Turkey. *Contributions to Mineralogy and Petrology*, 58, 63-81. https://doi.org/10.1007/BF00384745

Quandt, D., Trumbull, R., Altenberger, W., Cardona, A., Romer, R., Bayona, G., Ducea, M., Valencia, V., Vásquez, M., Cortés, E., & Guzmán, G. (2018). The geochemistry and geochronology of Early Jurassic igneous rocks from the Sierra Nevada de Santa Marta, NW Colombia, and tectono-magmatic implications. *Journal of South American Earth Sciences*, 86, 216-230. https://doi.org/10.1016/j.jsames.2018.06.019

Radelli, L. (1960). El basamento cristalino de la península de la Guajira. *Boletín Geológico*, 8 (1-3), 5-23.

Radelli, L. (1962). Acerca de la geología de la serranía de Perijá entre Codazzi y Villanueva (Magdalena-Guajira, Colombia). *Geología Colombiana*, 1, 23-42.

Renne, P. R., Swisher, C. C., Deino, A. L., Karner, D. B., Owens, T. L., & De Paolo, D. J. (1998). Intercalibration of standards, absolute ages and uncertainties in 40Ar/39Ar dating. *Chemical Geology*, 145 (1-2), 117-152. https://doi.org/10.1016/S0009- 2541(97)00159-9.

Restrepo, J. J., Ordóñez Carmona, O., Martens, U., Correa, A. M. (2009). Terrenos, complejos y provincias en la cordillera Central de Colombia. XII Congreso Colombiano de Geología.

Rodríguez, G., & Londoño, A. C. (2002). Mapa geológico del departamento de La Guajira. *Geología, recursos minerales y amenazas potenciales, Escala*, *1:250.000.* Bogotá: Ingeominas.

Rodríguez, G., Arango, M. I., Zapata, G., & Bermúdez, J. G. (2015). Características petrográficas, geoquímicas y edad U-Pb de los plutones jurásicos del valle superior del Magdalena. Poster. XV Congreso Colombiano de Geología.

Rodríguez, G., Arango, M. I., Zapata, G., & Bermúdez, J. G. (2016). Catálogo de unidades litoestratigráficas de Colombia, Formación Saldaña. Cordilleras Central y Oriental, Tolima, Huila, Cauca y Putumayo. Medellín: Servicio Geológico Colombiano.

Rodríguez, G., Zapata, G., Correa Martínez, A. M y Arango M. (2017). *Caracterización del magmatismo triásico-jurásico del macizo de Santander*. Medellín: Servicio Geológico Colombiano.

Rodríguez, G., Arango, M. I., Zapata, G., & Bermúdez, J. G. (2018). Petrotectonic characteristics, geochemistry, and U-Pb geochronology of Jurassic plutons in the Upper Magdalena Valley-Colombia: Implications on the evolution of magmatic arcs in the NW Andes. *Journal of South American Earth Sciences*, 81, 10-30. https://doi.org/10.1016/j.jsames.2017.10.012.

Rodríguez García, G., Correa Martínez, A. M., Zapata Villada, J. P., & Obando Erazo, G. (2019a). Fragments of a Permian arc on the western margin of the Neoproterozoic basement of Colombia. In: Gómez, J., & Mateus Zabala, D. (eds.), *The geology of Colombia*, vol. 1: *Proterozoic-Paleozoic*. Publicaciones Geológicas Especiales 35. Bogotá: Servicio Geológico Colombiano. https://doi.org/10.32685/ pub.esp.35.2019.10.

Rodríguez, G., Zapata Villada, J. P., Ramírez, D. A, Correa Martínez, A. M., Obando, G., Muñoz, J. A, Rayo, L., & Ureña, C. L. (2019b). *Magmatismo jurásico de la Sierra Nevada de Santa Marta*. Medellín: Servicio Geológico Colombiano.

Rodríguez, G., Correa Martínez, A. M., Zapata, G., Arango, M. I., Obando Erazo, G., Zapata Villada, J. P., & Bermúdez, J. G. (2020). Diverse Jurassic magmatic arcs of the Colombian Andes: Constraints from petrography, geochronology and geochemistry. In: Gómez, J., & Pinilla–Pachon, A.O. (eds.), *The Geology of Colombia*, vol. 2 Mesozoic. Publicaciones Geológicas Especiales 36. Bogotá: Servicio Geológico Colombiano. https://doi.org/10.32685/pub.esp.36.2019.04

Rubatto, D. (2002). Zircon trace element geochemistry: Partitioning with garnet and the link between U-Pb ages and metamorphism. *Chemical Geology*, 184 (1-2), 123-138. https://doi.org/10.1016/S0009-2541(01)00355-2.

Schoene, B., Samperton, K. M., Eddy, M. P., Keller, G., Adatte, T., Bowring, S. A., Khadri, S. F. R., & Gertsch, B. (2015). U-Pb geochronology of the Deccan Traps and relation to the end-Cretaceous mass extinction. *Science*, 347 (6218), 182-184. https://doi.org/10.1126/science.aaa0118

Shand, S. J. (1943). *Eruptive rocks: Their genesis, composition, classification, and their relation to ore-deposits with a chapter on meteorite.* New York: John Wiley & Sons.

Sláma, J., Košler, J., Condon, D. J., Crowley, J. L., Gerdes, A., Hanchar, J. M., Horstwood, M. S. A., Morris, G. A., Nasdala, L., Norberg, N., Schaltegger, U., Schoene, B., Tubrett, M. N., & Whitehouse, M. J. (2008). Plešovice zircon: A new natural reference material for U-Pb and Hf isotopic microanalysis. *Chemical Geology*, 249 (1-2), 1-35. https://doi.org/10.1016/j.chemgeo.2007.11.005.

Spikings, R., Cochrane, R., Villagómez, D., Van der Lelij, R., Vallejo, C., Winkler, W., & Beate, B. (2015). The geological history of Northwestern South America: From Pangaea to the early collision of the Caribbean Large Igneous Province (290-75 Ma). *Gondwana Research*, 27 (1), 95-139. https://doi.org/https://doi.org/10.1016/j.gr.2014.06.004.

Stacey, J. S., & Kramers, J. D. (1975). Approximation of terrestrial lead isotope evolution by a two-stage model. *Earth and Planetary Science Letters*, 26 (2), 207-221. https://doi.org/10.1016/0012-821X (75) 90088-6.

Streckeisen, A. (1978). IUGS Subcommission on the Systematics of Igneous Rocks: Classification and nomenclature of volcanic rocks, lamprophyres, carbonatites and melilitic rocks; recommendation and suggestions. *Neues Jahrbuch für Mineralogie - Abhandlungen*, 134, 1-14.

Sun, S. S., & McDonough, W. F. (1989). Chemical and isotopic systematics of oceanic basalts: Implications for mantle composition and processes. In: A. D. Sanders y M. J. Norry (eds.), *Magmatism in oceanic basins* (pp. 313-345). Special Publication 42. Oxford: Geological Society of London.

Trumpy, D. (1943). Pre-Cretaceous of Colombia. *GSA Bulletin*, 54, 1281-1304. https://doi.org/10.1130/GSAB-54-1281

Tschanz, C., Jimeno, A., & Cruz, J. (1969). *Geology of the Sierra Nevada de Santa Marta area, Colombia*. Informe interno n.º 1829. Bogotá: Ingeominas.

Tschanz, C. M., Marvin, R. F., Cruz B., J., Mehnert, H. H., & Cebula, G. T. (1974). Geologic evolution of the Sierra Nevada de Santa Marta, northeastern Colombia. *GSA Bulletin*, 85 (2), 273-284. https://doi.org/10.1130/0016-7606(1974)85<273:GEOTSN>2.0.CO;2

Villagómez, D. (2010). *Thermochronology, geochronology and geochemistry of the Western and Central Cordilleras and Sierra Nevada de Santa Marta, Colombia: The tectonic evolution of NW South America* (Ph. D. thesis). University of Geneva.

Villagómez, D., Martens, U., & Pindell, J. (2015). Are Jurassic and some older blocks in the Northern Andes in-situ or far-travelled? Potential correlations and new geochronological data from Colombia and Ecuador. Resumen, Conferencia Simposio: Tectónica Jurásica en la parte noroccidental de Suramérica y bloques adyacentes.

Weisbord, N. (1926). Venezuelan Devonian fossils. *Bulletins of American Paleontology*, 11 (46), 223-272.

Wiedenbeck, M., Allé, P., Corfu, F., Griffin, W. L., Meier, M., Oberli, F., Von Quadt, A., Roddick, J. C., & Spiegel, W. (1995). Three natural zircon standards for U-Th-Pb, Lu-Hf, trace element and REE analyses. *Geostandards Newsletter*, 19 (1), 1-23. https://doi.org/10.1111/j.1751-908X.1995.tb00147.x.

Wiedenbeck, M., Hanchar, J. M., Peck, W. H., Sylvester, P., Valley, J., Whitehouse, M.… Zheng, Y. F. (2004). Further characterisation of the 91500 zircon crystal. *Geostandards and Geoanalytical Research*, 28 (1), 9-39. https://doi.org/10.1111/j.1751-908X.2004.tb01041.x

Winchester, J. A., & Floyd, P. A. (1977). Geochemical discrimination of different magma series and their differentiation products using immobile elements. *Chemical Geology*, 20, 325-343. https://doi.org/10.1016/0009-2541(77)90057-2.

Woodhead, J. D., & Hergt, J. M. (2007). A Preliminary appraisal of seven natural zircon reference materials for in situ Hf isotope determination. *Geostandards and Geoanalytical Research*, 29, 183-195. https://doi.org/10.1111/j.1751-908x.2005.tb00891.x

Zapata García, G.; Rodríguez, G., & Arango, M. I. (2017). Petrografía, geoquímica y geocronología de rocas metamórficas aflorantes en San Francisco, Putumayo, y la vía Palermo-San Luis, asociadas a los complejos La Cocha-río Téllez y Aleluya. *Boletín Ciencias de la Tierra*, 41, 48-65. https://doi.org/10.15446/rbct.n41.58630

Zapata, S., Cardona, A., Jaramillo, C., Valencia, V., & Vervoort, J. (2016). U-Pb LA-ICP-MS geochronology and geochemistry of Jurassic volcanic and plutonic rocks from the Putumayo region (Southern Colombia): Tectonic setting and regional correlations. *Boletín de Geología*, 38 (2), 21-38. http://dx.doi.org/10.18273/revbol.v38n2-2016001

Zuluaga, C., Pinilla, A., & Mann, P. (2015). Jurassic silicic volcanism and associated continental-arc basin in Northwestern Colombia (Southern boundary of the Caribbean plate). In: C. Bartolini y P. Mann (eds.), *Petroleum geology and potential of the Colombian Caribbean margin*, AAPG memoir, vol. 108 (pp. 137-160). Tulsa: American Association of Petroleum Geologists.